Human Molecular Genetics, 2020, Vol. 29, No. 19 3165–3182

doi: 10.1093/hmg/ddaa172
Advance Access Publication Date: 8 August 2020
General Article

GENERAL ARTICLE

Assembly of the [4Fe–4S] cluster of NFU1 requires the coordinated donation of two [2Fe–2S] clusters from the scaffold proteins, ISCU2 and ISCA1

Anshika Jain, Anamika Singh, Nunziata Maio and Tracey A. Rouault*

Molecular Medicine Program, *Eunice Kennedy Shriver* National Institute of Child Health and Human Development, National Institutes of Health, Bethesda, MD 20892, USA

*To whom correspondence should be addressed. Tel: +1 3014967060; Email: rouault@mail.nih.gov

Abstract

NFU1, a late-acting iron–sulfur (Fe–S) cluster carrier protein, has a key role in the pathogenesis of the disease, multiple mitochondrial dysfunctions syndrome. In this work, using genetic and biochemical approaches, we identified the initial scaffold protein, mitochondrial ISCU (ISCU2) and the secondary carrier, ISCA1, as the direct donors of Fe–S clusters to mitochondrial NFU1, which appears to dimerize and reductively mediate the formation of a bridging [4Fe–4S] cluster, aided by ferredoxin 2. By monitoring the abundance of target proteins that acquire their Fe–S clusters from NFU1, we characterized the effects of several novel pathogenic NFU1 mutations. We observed that NFU1 directly interacts with each of the Fe–S cluster scaffold proteins known to ligate [2Fe–2S] clusters, ISCU2 and ISCA1, and we mapped the site of interaction to a conserved hydrophobic patch of residues situated at the end of the C-terminal alpha-helix of NFU1. Furthermore, we showed that NFU1 lost its ability to acquire its Fe–S cluster when mutagenized at the identified site of interaction with ISCU2 and ISCA1, which thereby adversely affected biochemical functions of proteins that are thought to acquire their Fe–S clusters directly from NFU1, such as lipoic acid synthase, which supports the Fe–S-dependent process of lipoylation of components of multiple key enzyme complexes, including pyruvate dehydrogenase, alpha-ketoglutarate dehydrogenase and the glycine cleavage complex.

Introduction

Iron–sulfur (Fe–S) clusters (ISCs) are ancient protein metallocofactors found in virtually all living organisms that are required for many fundamental biochemical processes, including respiration, DNA replication and heme biosynthesis. ISCs generally exist in two main forms: [2Fe–2S] and [4Fe–4S] clusters. These cofactors are assembled by a highly conserved and complex biochemical pathway that operates independently in the cytosol and mitochondria of mammalian cells (1,2). The current understanding of the molecular mechanisms of mitochondrial Fe–S protein biogenesis has been worked out in bacterial, yeast and human cells as well as in animal models. *De novo* generation of a basic rhombic [2Fe–2S] cluster occurs through assembly on a scaffold protein, ISCU, which has a mitochondrial (ISCU2) and a cytosolic/nuclear isoform (ISCU1) (3). The reaction requires sulfane sulfur, which is provided by the cysteine desulfurase (NFS1) aided by two ancillary proteins, ISD11 and ACP1 (4–7). It remains unclear how iron is provided to the nascent Fe–S cluster. Two other proteins that are important for the *de novo* assembly of the cluster on ISCU2 include frataxin (FXN), which is thought to regulate NFS1 activity (8), and ferredoxin2 (FDX2),

Received: April 24, 2020. **Revised:** July 9, 2020. **Accepted:** July 29, 2020

which is proposed to donate electrons for sulfur reduction (9–11). The newly assembled cluster is then transferred from ISCU2 to recipient proteins via multimolecular complexes composed of a chaperone/co-chaperone system and of intermediary transfer and secondary carrier proteins (1).

Multiple pathways for transfer of nascent clusters from ISCU2 to recipient proteins have been proposed. As elucidated in bacteria, yeast and human model systems, cluster release from mitochondrial ISCU to a subset of late-acting carrier proteins (12–14) is mediated by the ATPase activity of a chaperone (HSPA9 in humans) aided by a co-chaperone (HSC20 or HSCB in humans). HSC20 is thought to facilitate the transfer of the nascent Fe–S cluster from the scaffold protein to downstream carriers such as the monothiol glutaredoxin, GLRX5, found in the mitochondrial matrix (15,16) or directly to the target proteins such as SDHB (B subunit of succinate dehydrogenase) (12,17–19). GLRX5 is then proposed to heterodimerize with BOLA3 through shared bridging of a [2Fe–2S] cluster. Tetramerization of the BOLA3-GLRX5 dimers was recently shown *in vitro* to enable two [2Fe–2S] clusters to coalesce into a [4Fe–4S] cluster in the presence of reducing agents such as DTT and GSH, and the [4Fe–4S] cluster was subsequently transferred to downstream acceptors such as NFU1 (20). An alternative mechanism for [4Fe–4S] cluster formation proposed that the A-type ISC proteins, ISCA1 and ISCA2, and IBA57 received two [2Fe–2S] clusters from GLRX5 and assembled them into a [4Fe–4S] cluster that was transferred to NFU1 or BOLA3 or NUBPL (16,21). Recently, the assembly of a [4Fe–4S] cluster on ISCU *in vitro* and its direct transfer from the scaffold protein to purified NFU1 was also proposed, introducing yet another mechanism of [4Fe–4S] cluster assembly (22). Pathogenic mutations in NFU1, ISCA2, IBA57, BOLA3 and ISCA1 cause fatal infantile Multiple Mitochondrial Dysfunctions Syndrome (MMDS) types 1–5 (1,12,23). However, a clear pathway for Fe–S cluster transfer, likely mediated by these late-acting Fe–S cluster carriers (including ISCA proteins, NFU1, BOLA3 and GLRX5), from the primary scaffold to the target proteins *in vivo* has thus far remained elusive.

Studies in yeast and bacteria have characterized NFU1 as a non-essential, late-acting [4Fe–4S] cluster carrier protein (24,25). In these unicellular organisms, NFU1 appeared to play an essential role only under oxidative stress conditions. In humans, functional isoforms of NFU1 have been reported in both cytosol and mitochondria, and the purified NFU1 dimer has been shown to ligate a bridging [4Fe–4S] cluster (26–28). NFU1 is a bimodular protein, which contains two domains: a degenerate N-terminal domain (NTD) and a highly conserved C-terminal domain (CTD), which likely ligates the Fe–S cluster through its CXXC motif (26). The structures of both NTD-NFU1 and CTD-NFU1 were resolved by nuclear magnetic resonance (NMR) studies. Pathogenic mutations resulting in the depletion of functional NFU1 cause a rare infantile disease, Multiple Mitochondrial Dysfunctions Syndrome 1 (MMDS1) (29–32). The clinical symptoms usually include lactic acidosis, hyperglycinemia and reduced activities of mitochondrial respiratory complexes (29,30). Pulmonary hypertension and cardiomyopathy have also been reported in some of the patients with NFU1 mutations (29–31,33,34). Biochemical experiments on patient cells with NFU1 mutations have revealed decreased activities of several Fe–S cluster containing enzymes including lipoic acid synthase (LIAS), Complex-I (CI) and Complex-II (CII) (30,31). However, it remains unclear whether NFU1 directly delivers [4Fe–4S] clusters to a subset of recipient proteins or if it indirectly mediates Fe–S cluster transfer to downstream secondary carriers, which then transfer Fe–S clusters to recipient apo-proteins. The mechanism by which NFU1 acquires its Fe–S cluster *in vivo* has also thus far remained unknown. In this study, we report that NFU1 interacts directly with the main scaffold protein ISCU2 and with ISCA1 through a conserved hydrophobic motif to dimerize and build its [4Fe–4S] cluster. Dimerization enables NFU1 to assemble a [4Fe–4S] cluster when the two [2Fe–2S] clusters from each Fe–S donor, namely ISCU2 and ISCA1, coalesce to generate a [4Fe–4S] cluster that bridges the dimer, aided by the likely contribution of reducing equivalents from FDX2. Additionally, NFU1 appears to be a major carrier of [4Fe–4S] clusters, which is able to engage, through direct physical interaction, with a partially defined subset of target apo-proteins to deliver [4Fe–4S] clusters to recipient proteins, including LIAS and SDHB.

Results

A [4Fe–4S] cluster ligating human NFU1 interacted with the main mitochondrial Fe–S cluster scaffold protein ISCU2

A dimer of NFU1 has been reported to ligate a [4Fe–4S] cluster *in vitro* likely via the two conserved cysteine residues (C_{210} and C_{213}) present at the C-terminus of each monomer (26–28). To validate this observation *in vivo*, we overexpressed and purified human NFU1 and the $NFU1^{C210A\_C213A}$ mutant in which the two cysteines were replaced by alanines from *Escherichia coli* cells that co-expressed the ISC operon from *Azotobacter vinelandii* (Fig. 1A). As shown in Figure 1B, the as-purified NFU1-WT protein showed a broad shoulder at 425 nm, a distinctive feature of [4Fe–4S] cluster, which was clearly missing from the mutant $NFU1^{C210A\_C213A}$ (Fig. 1B). Furthermore, the $NFU1^{C210A\_C213A}$ mutant was unable to ligate the cluster even upon *in vitro* chemical reconstitution ($Rc\_NFU1^{C210A\_C213A}$) (Fig. 1B). These results confirmed that NFU1 ligated a [4Fe–4S] cluster *in vivo* as a dimer via its conserved cysteine residues (C_{210} and C_{213}) on each monomer.

To establish the position of NFU1 in the sequence of events that lead to Fe–S cluster biogenesis/transfer and to determine whether it functioned as a late-acting carrier protein that acquired its cluster from intermediary chaperones or directly acquires its Fe–S cluster from the initial mitochondrial Fe–S cluster scaffold protein (ISCU2), we examined its potential direct interacting partners among the candidate ISC biogenesis proteins (ISCU2, NFU1, ISCA1, ISCA2, IBA57, FDX2, GLRX5, BOLA3) by yeast two-hybrid (Y2H) assay. Our results revealed that NFU1 interacted directly with NFU1, ISCU2, ISCA1 and FDX2 (Fig. 1C). While the interaction between NFU1-bait and NFU1-prey was consistent with the already known ability of NFU1 to dimerize, the interaction of NFU1 with the electron donor, FDX2, and the two scaffold proteins ISCU2 and ISCA1 (Fig. 1C) suggested the possibility that assembly of the [4Fe–4S] cluster on NFU1 required acquisition of two [2Fe–2S] clusters, each donated by ISCU2 and ISCA1, which coalesced through reductive coupling into a [4Fe–4S] cluster, utilizing electrons provided by FDX2 (9,15,35).

We also detected direct interaction of ISCU2 with NFU1, ISCA1, FDX2 and GLRX5 (Fig. 1C). These results suggest that NFU1, ISCA1 and GLRX5 may independently acquire their clusters directly from ISCU2 before diverging to serve their target proteins. Additionally, we tested the interaction of NFU1 with its two proposed target proteins, SDHB and LIAS (30,31), and observed direct interactions between NFU1 and SDHB as well as LIAS via the Y2H assay (Fig. 1D). Remarkably, the interaction of NFU1 with its targets was observed under highly stringent conditions, with 3-AT concentrations as high as 2 mM, whereas its

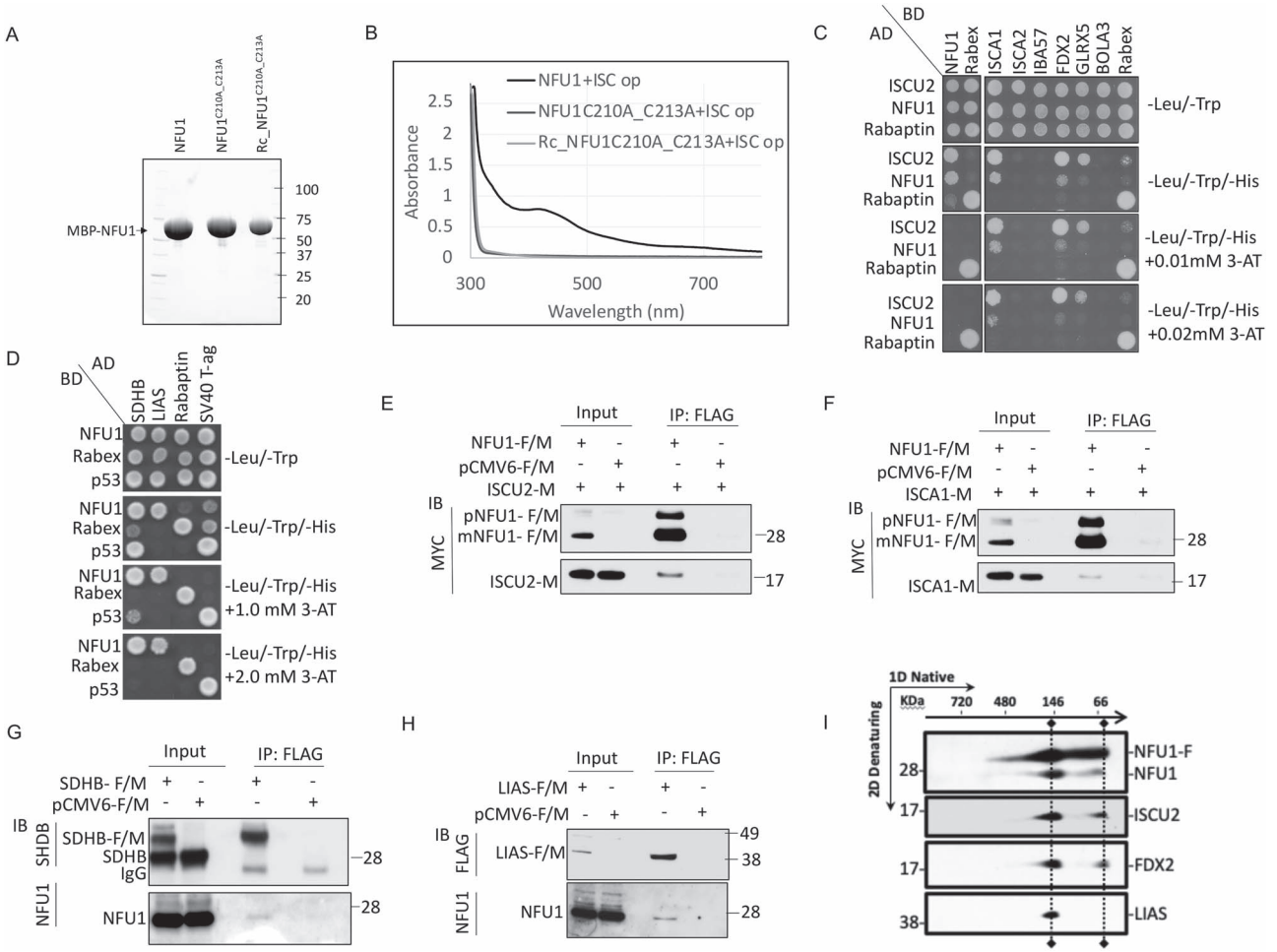

Figure 1. Mammalian NFU1 ligates a [4Fe–4S] cluster and directly interacts with ISCU2. (**A**) SDS-PAGE separation of the purified proteins on a stain-free denaturing gel. (**B**) UV–visible spectra of as-purified MBP-NFU1, MBP-NFU1^{C210_C213A} and chemically reconstituted-Rc_MBP-NFU1^{C210_C213A} proteins from *E. coli* co-expressing the ISC operon from *A. vinelandii*. The MBP-tagged proteins were purified using amylose resin affinity purification followed by the HiTrap Q column ion-exchange purification. ISC, Iron-Sulfur Cluster; Op, operon; Rc, chemically reconstituted. (**C** and **D**) Y2H assays. (C) Prey vectors expressing GAL4-AD fused with ISCU2, NFU1 or Rabaptin were co-expressed with the bait vectors expressing GAL4-BD fused with NFU1, ISCA1, ISCA2, IBA57, FDX2, GLRX5, BOLA3 or Rabex, as indicated in AH109 yeast cells. Direct interactions between preys and baits were tested by Y2H assay in -Leu/-Trp/-His media. 3-AT, a competitive inhibitor of HIS3, was used to increase the stringency of the assay. (D) SDHB, LIAS, Rabaptin or SV40-T-Ag, each cloned in the prey vector, were co-transformed with NFU1, RABEX5 or p53 in the bait vector in AH109 yeast cells and tested for direct interactions via Y2H assay. (**E** and **F**) Total cell lysates from HeLa cells co-transfected with (E) pCMV6-NFU1-F/M + ISCU2-M or pCMV6-F/M + ISCU2-M or (F) pCMV6-NFU1-F/M + ISCA1-M or pCMV6-F/M + ISCA1-M were subjected to IP with anti-FLAG beads (mouse) followed by immunoblot (IB) with anti-MYC (rabbit). (**G** and **H**) Total cell lysates from *HeLa* cells transfected with (G) pCMV6-SDHB-F/M or (H) pCMV6-LIAS-F/M were subjected to IP with anti-FLAG beads (mouse) followed by IB with anti-NFU1 (rabbit), anti SDHB (mouse) or anti-FLAG (rabbit). Total cell lysates expressing the empty vector (pCMV6-F/M) were used as controls. The input loaded on the gel is a small fraction (5–10%) of the total sample loaded for IP, and therefore, an enrichment of the FLAG-tagged proteins is observed in the IP samples. (**I**) 2D native/SDS-PAGE immunoblots identified two NFU1-containing complexes isolated from mitochondrial extracts of HEK293 cells transfected with FLAG-tagged NFU1. Abbreviations: pNFU1-F/M: FLAG and MYC tagged precursor-NFU1 (1–254); mNFU1-F/M: FLAG and MYC tagged mature mitochondrial isoform of NFU1; NFU1-F: FLAG-tagged NFU1.

interactions with ISCU2 and ISCA1 were detected only on plates with negligible amounts of 3-AT, suggesting that the affinity of the interaction between NFU1 and either ISCU2 or ISCA1 was low, as expected for a transient interaction (36). Although it is possible that the interactions of apo-NFU1 (likely a less stable form) with ISCU2 and ISCA1 are weak and transient as opposed to its interaction with the targets when NFU1 has been stabilized by the [4Fe–4S] cluster, it is also plausible that the interaction of NFU1 with an individual donor (ISCU2 or ISCA1) that appears weak in the binary setting of the Y2H assay could be strengthened if the donor proteins were present as a complex with the right ancillary/partner protein, and therefore, the strength of the interaction of NFU1 with its donors or targets may be different *in vivo*. The binding affinities between the interacting proteins are a subject for further investigation.

Co-immunoprecipitation (co-IP) assays in mammalian cells confirmed these interactions between Fe–S donors and NFU1 and the NFU1 targets *in vivo* (Fig. 1E–H and Supplementary Material, Fig. S1A–C). The interactions between NFU1 and ISCU2 (Fig. 1E and Supplementary Material, Fig. S1A) and between NFU1 and ISCA1 (Fig. 1F and Supplementary Material, Fig. S1B) were confirmed by reciprocal co-IP experiments. Similarly, reciprocal co-IP experiments validated the interaction of NFU1 with two target proteins, SDHB (Fig. 1G and Supplementary Material, Fig. S1C) and LIAS (Fig. 1H and Supplementary Material, Fig. S1D), in the mammalian cells. Moreover, by analyzing the protein complexes that co-immunoprecipitated with FLAG-tagged NFU1 (NFU1-F) by 2D native/SDS-PAGE, we were able to characterize the composition of two main complexes containing mitochondrial NFU1 *in vivo* (Fig. 1I). The lower molecular weight

(MW) complex that had an apparent MW of 66 kDa on the native gel (first dimension) contained endogenous NFU1, which confirmed that NFU1 dimerized *in vivo*, and also bound ISCU2 and FDX2. Although we were unable to detect ISCA1 in the complex, due to the low sensitivity of the anti-ISCA1 antibody, the direct interaction observed between NFU1 and ISCA1 in Y2H and mammalian co-IP experiments (Fig. 1C and F and Supplementary Material, Fig. S1B) suggests that ISCA1 co-exists along with an NFU1 dimer, ISCU2 and FDX2 in a quaternary complex. A second complex of higher MW (~146 kDa) contained LIAS in addition to the components detected in the complex at ~66 kDa. The co-existence of LIAS with NFU1 and the Fe–S cluster scaffold, ISCU2, in a single complex suggests that the assembly and transfer of the [4Fe–4S] cluster from NFU1 occur almost contemporaneously, thereby likely protecting the Fe–S cluster from degradation by cellular oxidants during the assembly and transfer process. Interestingly, FDX2 was found to associate with the complex at ~146 kDa (Fig. 1I). The presence of FDX2 in this complex may be required to enable the reductive coupling of the two [2Fe–2S] clusters donated by ISCU2 and ISCA1 into the [4Fe–4S] ligated by NFU1. Another interesting possibility for the presence of FDX2 in the higher MW complex comes from studies in bacteria that reported the association of bacterial ferredoxins with the S-adenosyl-methionine (SAM) [4Fe-4S] cluster in the prokaryotic radical SAM enzyme MiaB, in order to maintain the cluster in the catalytically active +1 oxidation state (37–40). FDX2 may perhaps donate one electron to the SAM-ligating $[4Fe–4S]^{2+}$ of LIAS to reduce it to $[4Fe–4S]^{+1}$. Taken together, these results demonstrate that NFU1, which ligates a [4Fe–4S] cluster, interacted with two potential Fe–S cluster donors, ISCU2 and ISCA1, with the electron donor, FDX2, and with two Fe–S recipient proteins, SDHB and LIAS.

NFU1 interacted with ISCU2 via a hydrophobic domain identified by site-directed mutagenesis

To map the site of interaction with its potential Fe–S cluster donor proteins on NFU1, we used mutational/deletional analysis approaches in conjunction with Y2H screens. We first investigated the site of interaction between NFU1 and ISCU2. To identify the domain of NFU1 involved in the interaction with ISCU2, the constructs encoding NTD-NFU1 (25–150) and CTD-NFU1 (150–254) along with the full-length NFU1 (25-254) were tested in Y2H assays. Consistent with the previous observations (22), we detected a strong interaction between ISCU2 and NFU1 mediated by its CTD but not its NTD (Fig. 2A). Similarly, only CTD-NFU1 and not NTD-NFU1 appeared to dimerize with NFU1 (Supplementary Material, Fig. S2A), which argued against the possibility of formation of a holo-NFU1 oligomer mediated by its NTD residues (26). Deletion of the NTD from NFU1 appeared to strengthen the interaction of the CTD of NFU1 with ISCU2, likely because the NTD caused steric hindrance. Thus, our data suggest that the NTD may contribute to the transient nature of the interaction between NFU1 and ISCU2. In contrast, the target protein, SDHB, interacted strongly with both the NTD and CTD of NFU1 (Fig. 2A). Interestingly, LIAS interacted only with specific conserved residues of CTD-NFU1 (Supplementary Material, Fig. S2B), unlike the bacterial homologue NfuA, which has a unique NTD that differs significantly from human NFU1 (41). To summarize, these results suggest that the Fe–S cluster ligating CTD of NFU1 physically interacted with both the Fe–S cluster donor and recipient proteins.

We then performed extensive mutational analysis of several conserved residues and peptide sequences in the CTD of NFU1. A comprehensive Y2H screening of the mutants revealed that a surface-exposed, hydrophobic motif, consisting of F_{230} and Y_{231}, mediated an interaction between CTD-NFU1 and ISCU2 (Supplementary Material, Figs S2C–E and S3). Additionally, the polar residue N_{226} also appeared to be important for this interaction (Supplementary Material, Fig. S2D). The double mutation of F230A_Y231A on CTD-NFU1 completely abrogated the interaction between NFU1 and ISCU2. In contrast, the interaction with the recipient protein, SDHB, was not affected (Fig. 2B). Additionally, the double mutations, C210A_C213A, did not affect the interaction of NFU1 with either ISCU2 or SDHB, indicating that the site for cluster ligation (CXXC) is distinct from the site that mediates initial cluster acquisition (FY) by NFU1 (Fig. 2B and C).

When the effect of these mutations on the interaction of NFU1 with ISCU2 was measured *en bloc* in HeLa cells, similar results were observed. While $NFU1^{C210A\_C213A}$ and $NFU1^{N226A\_M227A}$ interacted with ISCU2 similar to the WT-NFU1; $NFU1^{F230A\_Y231A}$ exhibited a significant loss of interaction with ISCU2 (Fig. 2D). We tested the effects of N226A and M227A mutations separately and found that the substitution of either of these two residues individually resulted in a stronger interaction between NFU1 and ISCU2 (Fig. 2E), suggesting that N_{226} and M_{227} may contribute to the transient nature of this interaction, perhaps because their polarity diminished affinity. Taken together, these results suggest that the residues $N_{226}M_{227}$ appeared to play an important indirect role in maintaining the transient nature of the interaction between NFU1 and ISCU2, whereas the $F_{230}Y_{231}$ motif of NFU1 was involved in a direct interaction with ISCU2 (Fig. 2C).

Reciprocally, the major molecular determinants of the CTD-NFU1/ISCU2 interaction were also identified on the primary scaffold ISCU2 using deletional/mutational analyses of conserved residues on ISCU2 in conjunction with Y2H assays. Six residues (V_{72}, M_{73}, V_{79}, G_{83}, F_{90} and F_{94}) on three different peptides of ISCU2 were found to play a significant role in its interaction with CTD-NFU1 (Fig. 3A and B). Interestingly, four of these residues (namely, V_{72}, M_{73}, F_{90} and F_{94}) have been previously identified as being involved in the mutually exclusive interaction of ISCU2 with either the cysteine desulfurase NFS1 or with the co-chaperone Jac1, the yeast ortholog of HSC20 (13). The residues on Peptide #2 of ISCU2 (comprising amino acid residues V_{79}-G_{83}) appeared to be far from the Fe–S cluster binding site on the main scaffold and thus might contribute to anchoring the NFU1 dimer to ISCU2 (Fig. 3B). Nevertheless, the site of interaction of ISCU2 with NFU1 appeared to be positionally advantageous for the transfer of the Fe–S cluster to the interacting NFU1 protein (Fig. 3C).

The ISCA1 binding site on NFU1 overlapped with the binding site for ISCU2

We then investigated the potential involvement of the FY motif of NFU1 in its interactions with the other binding partners identified in our study, ISCA1 and FDX2 (Fig. 1 and Supplementary Material, Fig. S1). The Y2H screening on the NFU1 mutants ($NFU1^{F230A\_Y231A}$ and $NFU1^{C210A\_C213A}$) revealed that while these mutations had no effect on the interaction of NFU1 with FDX2, they impaired the interaction between NFU1 and ISCA1 (Fig. 4A). Similar observations in mammalian cells by co-IP experiments confirmed that the loss of $C_{210}\_C_{213}$ as well as $F_{230}\_Y_{231}$ motifs of NFU1 significantly inhibited its interaction with ISCA1 *in vivo* (Fig. 4B). Interestingly, the substitution of $N_{226}M_{227}$ residues (which influenced binding to ISCU2) into alanines did not affect the interaction of NFU1 with ISCA1 (Fig. 4B). Overall, these results indicated that ISCA1 interacted

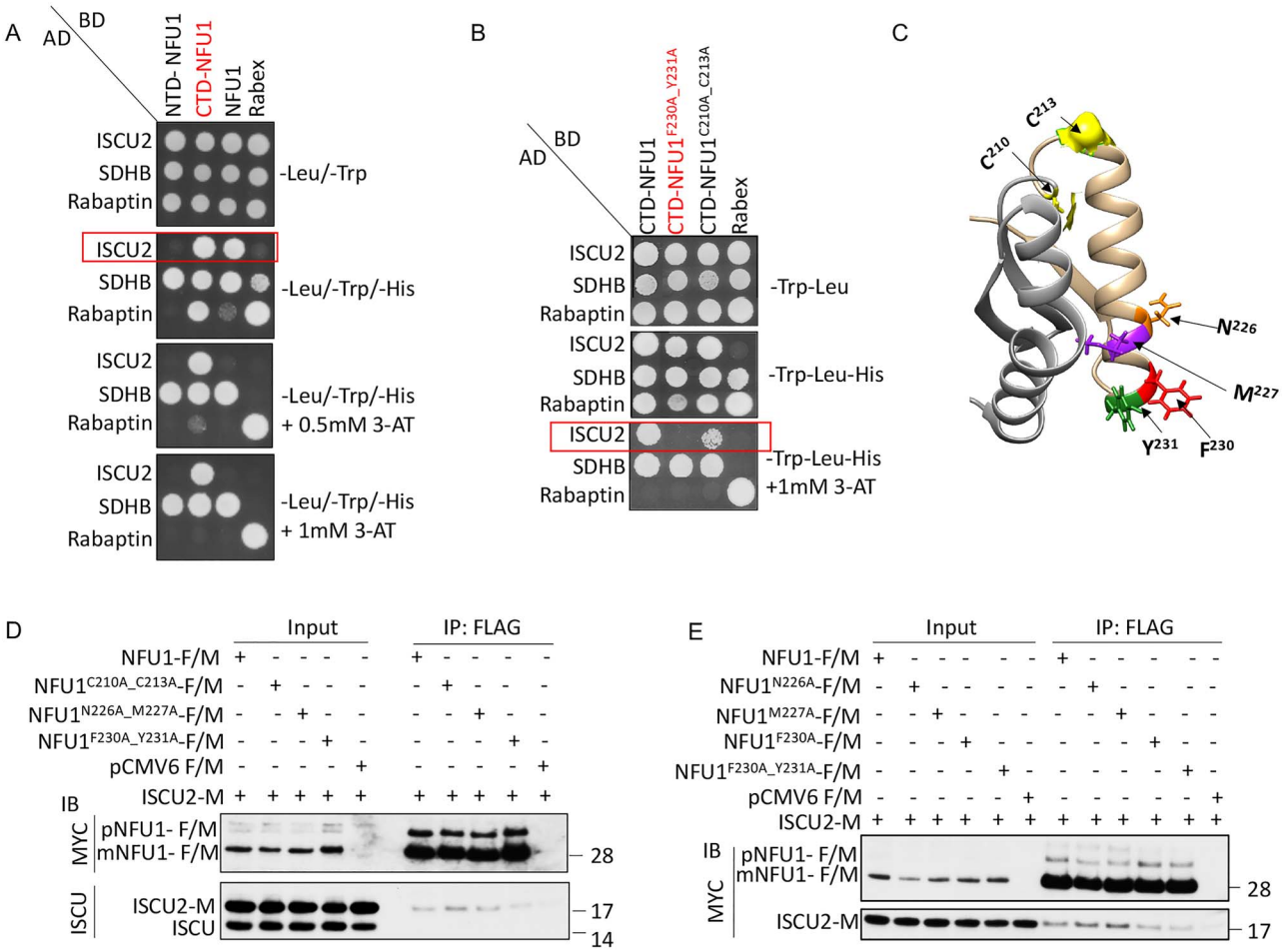

Figure 2. NFU1 interacts with ISCU2 via a hydrophobic FY motif in its CTD. (**A**) NTD-NFU1 (25–150), CTD-NFU1 (150–254; highlighted in red) and NFU1 (25–254) were cloned into the bait vector and assayed for a direct interaction with ISCU2 or SDHB cloned in the prey vector via Y2H assay. (**B**) Y2H assay to test the interaction between baits (CTD-NFU1, NFU1^{F230A_Y231A} (highlighted in red), NFU1^{C210A_C213A} or Rabex) and preys (ISCU2, SDHB or Rabaptin). The red boxes highlight the distinct interaction patterns of the baits with ISCU2-prey. Rabex and Rabaptin were used as controls. 3-AT, a competitive inhibitor of HIS3, was used to increase the stringency of the assay. (**C**) Ribbon representation of the NMR structure of CTD-NFU1 (PDB: 2M5O) highlighting the residues (F_{230}, Y_{231}, N_{226}, M_{227}) involved in its interaction with ISCU2. Cysteines C_{210} and C_{213} that ligate the [4Fe–4S] cluster are shown in yellow. CTD-NFU1 (150–211) and CTD-NFU1 (212–254) are represented in grey and tan, respectively. (**D** and **E**) HeLa cell extracts co-expressing ISCU2-M and NFU1-F/M or alanine mutants of NFU1-F/M or the empty vector (pCMV6) were immunoprecipitated with anti-FLAG beads (mouse) and immunoblotted with anti-MYC (rabbit) or anti-ISCU (rabbit) antibodies. The input loaded on the gel is a small fraction (5–10%) of the total sample loaded for IP, and therefore, an enrichment of the FLAG-tagged precursor (pNFU1) and mitochondrial NFU1 (mNFU1) bands is observed in the IP samples. These figures are a representative of a result that was obtained at least three times.

with NFU1 at the same hydrophobic site (F_{230}_Y_{231}) as ISCU2, suggesting that this motif of NFU1 functioned in engaging its two potential donors, namely ISCU2 and ISCA1, each able to interact with an NFU1 monomer of the dimeric functional [4Fe–4S]-NFU1 through binding to the FY motif. Additionally, the loss of interaction between ISCA1 and NFU1^{C210A_C213A} mutant suggests the possibility that ligation of the Fe–S cluster between the ISCA1 and NFU1 heterodimer may stabilize the interaction between these two proteins, as was previously reported for the bacterial heterodimer formed by the A-type carrier ErpA and NfuA (42). Alternatively, it is possible that ISCA1 is recruited by NFU1 once the C_{210} and C_{213} of NFU1 are engaged in ligating a Fe–S cluster.

Human [2Fe–2S] cluster-ISCA1 is required for cluster formation on NFU1

To address whether the interaction between [2Fe–2S]-ISCA1 and NFU1 was physiologically relevant for cluster acquisition by NFU1, we first investigated the stoichiometry of the Fe–S cluster ligated by human ISCA1. We co-expressed full-length human ISCA1-MBP with the ISC operon and purified the protein anaerobically from *E. coli*. The as-purified ISCA1-MBP protein eluted as a single band in a brown colored solution (Fig. 5A and B), which showed the UV–visible spectrum (a peak at 320 as well as 420 nm) characteristic of [2Fe–2S] clusters (Fig. 5C), as was observed previously for the murine ISCA1 and (43). These results support that human ISCA1 is a [2Fe–2S] cluster ligating protein.

Subsequently, to determine if the [2Fe–2S] cluster bound ISCA1 was a physiological Fe–S cluster donor to NFU1, we monitored the effect of loss of *IscA* (the bacterial homologue of ISCA1) on cluster acquisition by overexpressing the recombinant human NFU1 in *E. coli* cells that overexpressed the ISC operon. Accordingly, we modified the ISC operon from *A. vinelandii* by making an in-frame deletion of the *IscA* gene from the operon (del-IscA Op) and then co-expressing it with human NFU1 (MBP-NFU1) in *E. coli*. Cultures of MBP-NFU1 co-expressed

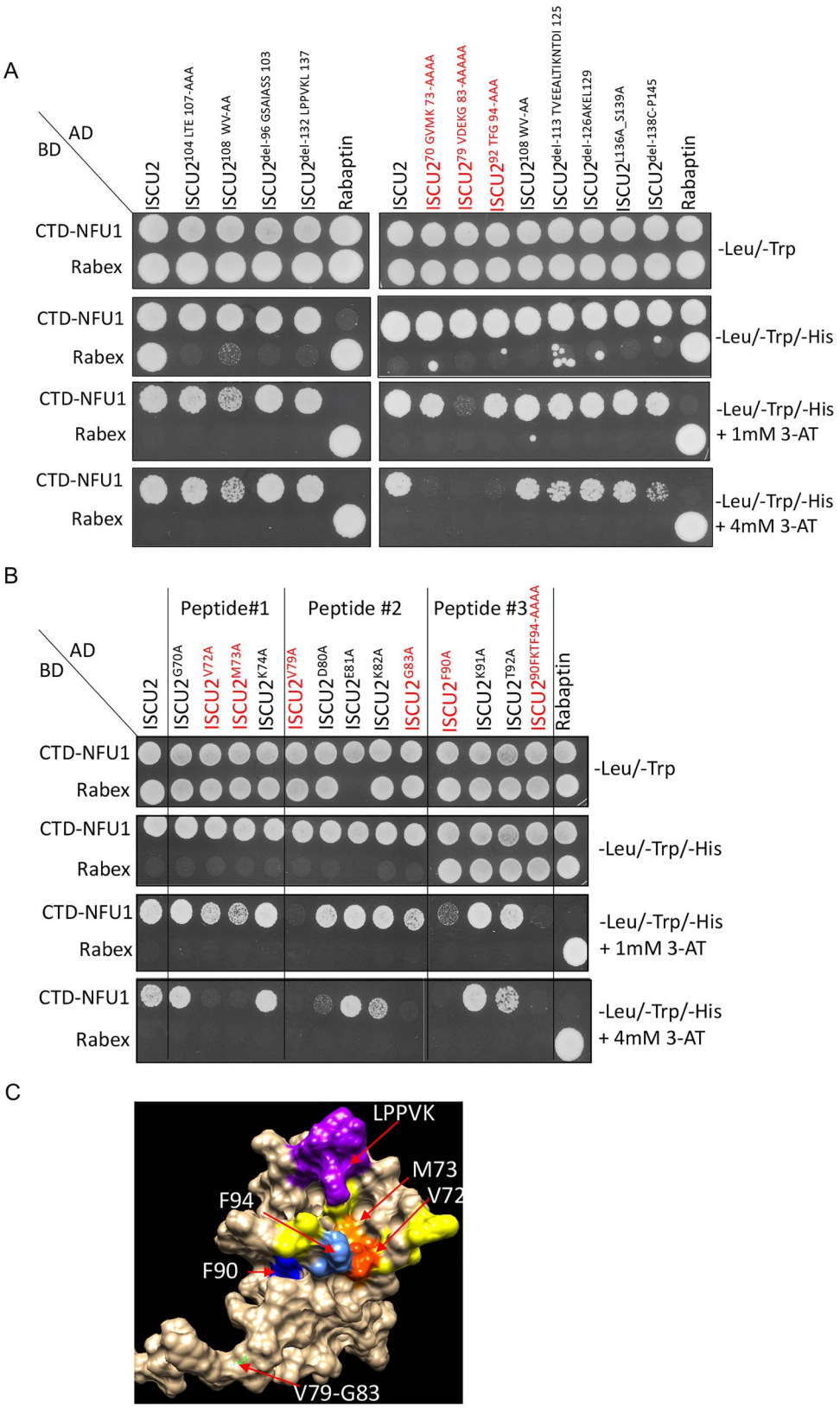

Figure 3. Identification of the amino acid residues on ISCU2 involved in its interaction with NFU1. (**A**) Mutational and deletional analyses of several stretches on ISCU2 protein sequence yielded three conserved peptides that showed interaction with CTD-NFU1 by Y2H assay. (**B**) Mutagenesis of individual amino acids present on the three peptides of the protein that were identified to interact with CTD-NFU1 using Y2H assay. ISCU2 mutants shown in red indicate the amino acids involved in its interaction with CTD-NFU1. CTD-NFU1 and Rabex were cloned into the bait vector and ISCU2 and Rabaptin were cloned into the prey vector. Rabaptin-Prey and Rabex-Bait were used as controls. (**C**) Surface representation of the NMR structure of ISCU2 (PDB: 2L4X) highlighting the residues involved in its interaction with NFU1 (red: V72, orange: M73, green: V79-G83, deep blue: F90, corn blue: F94) , the Fe–S cluster ligating residues (yellow) and the LPPVK motif (purple), which is the binding site for HSPA9.

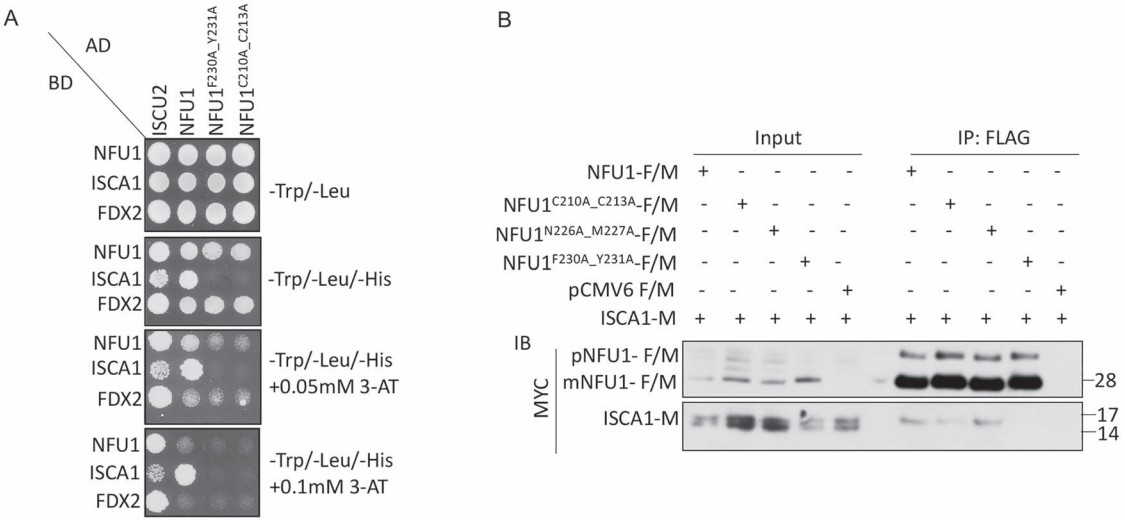

Figure 4. ISCA1 interacts with NFU1 via the same hydrophobic motif (F_{230}_Y_{231}) that mediated the interaction between NFU1 and ISCU2 and also requires C210_C213. (**A**) Alanine mutants of NFU1 ($NFU1^{F230A\_Y231A}$, $NFU1^{C210A\_C213A}$) along with full-length NFU1 and ISCU2 cloned in the prey vector were assessed for an interaction with full-length NFU1, ISCA1 or FDX2 cloned in the bait vector via Y2H assay. (**B**) HeLa cell extracts co-expressed with ISCA1-M and NFU1-F/M or alanine mutants of NFU1-F/M or the empty vector (pCMV6-F/M) were immunoprecipitated with anti-FLAG beads (mouse) and immunoblotted with anti-MYC antibody (rabbit). The input loaded on the gel is a small fraction (5–10%) of the total sample loaded for IP, and therefore, the FLAG-tagged precursor (pNFU1) and mitochondrial NFU1 (mNFU1) bands are enriched in the IP samples. The co-IP data presented here are a representative of results that were obtained at least three times.

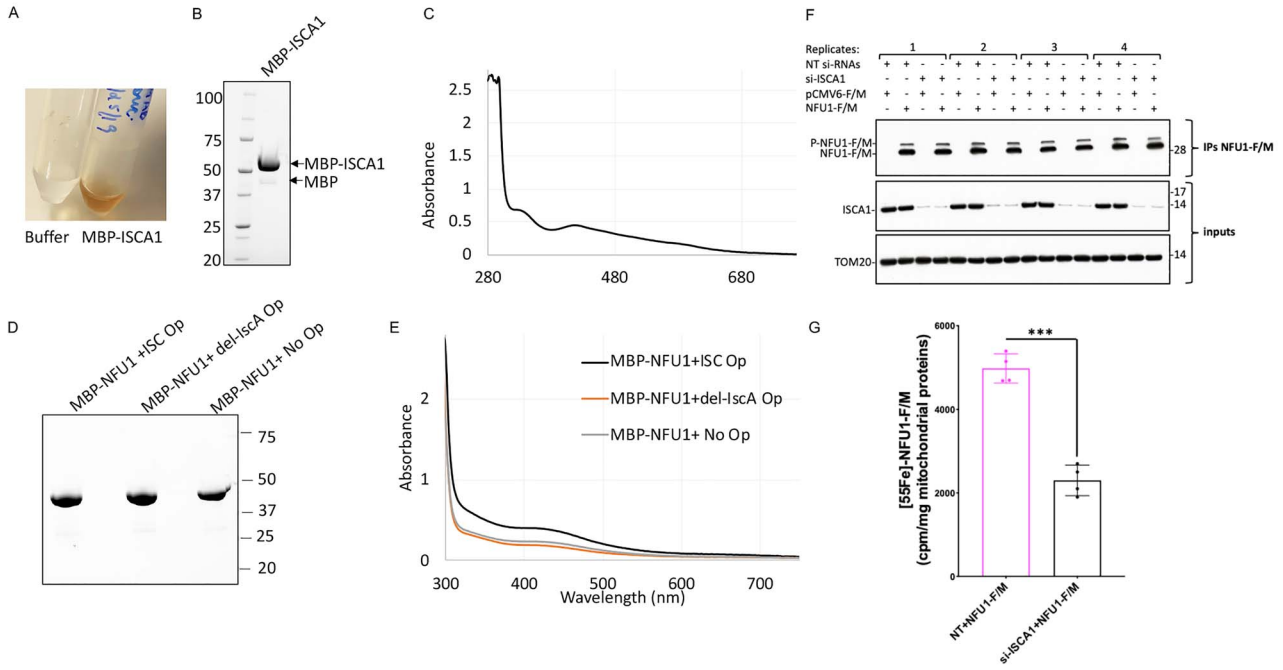

Figure 5. Human ISCA1 ligates a [2Fe–2S] cluster and is required for cluster formation on NFU1. (**A**) The as-purified MBP-ISCA1 protein from *E. coli* co-expressing the ISC operon from *A. vinelandii* eluted as a brown colored solution from the amylose resin. (**B**) SDS-PAGE separation of purified MBP-ISCA1 protein on a stain-free denaturing gel. (**C**) UV–visible spectrum of as-purified MBP-ISCA1 shows the characteristic features of a [2Fe–2S] cluster (43). (**D**) SDS-PAGE separation and (**E**) UV–visible spectrum of MBP-NFU1 purified from *E. coli* co-expressing either WT ISC operon (ISC Op), ISC operon with deleted IscA (del-IscA Op) or no operon (No Op) on a stain-free denaturing gel. The MBP-tagged proteins were purified using amylose resin affinity purification followed by the HiTrap Q column ion-exchange purification. (**F**) IBs on samples as those analyzed in (**G**) for the 55Fe incorporation into NFU1-F/M showed effective knockdown of *ISCA1* in mammalian cells transfected with siRNAs targeting the *ISCA1* mRNA and efficient immunoprecipitation of recombinant NFU1-F/M. TOM20 was used as a loading control (G) ^{55}Fe incorporation into NFU1-F/M assessed by liquid scintillation counting showed significantly decreased levels of radioactive iron incorporated into NFU1-F/M upon KD of ISCA1. The background, corresponding to ^{55}Fe measurements of eluates after anti-FLAG immunoprecipitations on mitochondrial extracts from cells transfected with the empty vector, was subtracted from each reading. Unpaired *t*-test analyses of ^{55}Fe labeling experiments were performed with GraphPad Prism 7. ***$P < 0.001$.

with (+ISC Op) or without (No Op) the ISC operon were used as positive and negative controls, respectively. Highly pure MBP-NFU1 proteins were anaerobically purified from all three bacterial cell lysates (Fig. 5D). Interestingly, the UV–visible spectrum of MBP-NFU1 purified from cells expressing the ISC operon lacking *IscA* (IscA-del Op) showed similar cluster occupancy as the MBP-NFU1 purified from cells without the operon, which was ~50% lower than the levels of cluster occupancy of NFU1 purified from cells expressing the WT-ISC operon (Fig. 5E). The residual cluster occupancy observed in the spectrum of NFU1 purified in the absence of the operon or in the IscA-del Op cells was likely to have been contributed by the endogenous ISC proteins of *E. coli*. These results suggest that IscA is required for cluster acquisition by NFU1 *in vivo* in *E. coli*. We did not perform the deletion of the main scaffold *IscU* from the ISC operon as it is essential for Fe–S cluster assembly (44–46).

To confirm the role of ISCA1 as the Fe–S cluster donor to NFU1 in mammalian cells, we examined ^{55}Fe-incorporation by NFU1 in cells in which *ISCA1* expression had been silenced. HEK293 cells cultured in the presence of ^{55}Fe-Tf were transfected with small interfering RNAs (siRNAs) targeting *ISCA1* mRNA to knockdown its expression and co-transfected at the time of the second transfection with siRNAs against ISCA1 with either NFU1-F/M or pCMV6-Entry plasmids. The incorporation of ^{55}Fe on immunoprecipitated NFU1-F/M from control or *ISCA1* knock down cell lines was then measured by liquid scintillation counting. We observed a 54% decrease in the ^{55}Fe signal associated with NFU1-F/M immunoprecipitated from *ISCA1* knockdown cells as opposed to control, supporting that ISCA1 was involved in Fe–S cluster donation to NFU1 (Fig. 5F and G).

NFU1$^{FY\text{-}AA}$ mutant was unable to acquire the [4Fe–4S] cluster from the donor proteins

To investigate if the FY motif (F_{230}_Y_{231}) of NFU1 that mediated its interaction with ISCU2 and ISCA1 was in fact necessary for the Fe–S cluster acquisition by NFU1, we purified MBP-NFU1 and MBP-NFU1$^{FY\text{-}AA}$ mutant anaerobically from *E. coli* co-expressing the ISC operon (Fig. 6A). As opposed to the WT-NFU1, the NFU1$^{FY\text{-}AA}$ mutant lacked the brown color (Fig. 6B) as well as the shoulder around 425 nm as observed on the UV–visible spectrum of WT-NFU1, indicating the absence of a [4Fe–4S] cluster on the NFU1$^{FY\text{-}AA}$ mutant (Fig. 6C). To determine if the absence of cluster ligation on NFU1$^{FY\text{-}AA}$ mutant was in fact due to its inability to acquire Fe–S clusters from its physiological donors, we performed *in vitro* chemical reconstitution of the cluster on apo-NFU1 and apo-NFU1$^{FY\text{-}AA}$. Both WT and NFU1$^{FY\text{-}AA}$, after chemical reconstitution, showed the shoulder at 425 nm, which is a characteristic feature of a [4Fe–4S] cluster, on their UV–visible spectrum (Fig. 6D and E). These results suggest that while NFU1$^{FY\text{-}AA}$ was able to ligate a [4Fe–4S] cluster *in vitro*, the FY motif on NFU1 was important for the physiological acquisition of the Fe–S cluster from the biogenesis machinery *in vivo*. Additionally, we purified the NFU1$^{NM\text{-}AA}$ mutant and observed a slightly lower cluster occupancy than the WT on the as-purified mutant protein (Fig. 6F and G). Taken together, these data suggest that the NM motif (N_{226}_M_{227}), which indirectly participated in the interaction of NFU1 with ISCU2, also contributed to the cluster acquisition by NFU1. Furthermore, the FY motif of NFU1, which mediated direct interactions with both ISCU2 and ISCA1, was essential for the *in vivo* Fe–S cluster acquisition from these donors.

Complementation with WT-NFU1 restored the biochemical defects of NFU1-deficient patient cells whereas complementation with either NFU1$^{FY\text{-}AA}$ or NFU1$^{NM\text{-}AA}$ did not

NFU1 is believed to serve as a [4Fe–4S] cluster carrier for several mitochondrial proteins including SDHB and LIAS (30), and the defects in NFU1 have been shown to result in biochemical defects such as reduced activities of CI, CII and LIAS. Based on the direct interactions observed between NFU1 and SDHB/LIAS and the defects displayed by NFU1$^{FY\text{-}AA}$ and NFU1$^{NM\text{-}AA}$ mutants in the cluster acquisition, we speculated that these mutants would mirror the NFU1-deficiency phenotype resulting in loss of SDHB and LIAS activities. To investigate the *in vivo* effects of NM-AA and FY-AA substitutions on the function of NFU1, we used a previously characterized NFU1 patient-derived fibroblast cell line (NFU1 Pt: c.545G>A (p.Arg182Gln)) (30) and assessed the levels of various Fe–S cluster containing proteins upon complementation with either the WT (+NFU1-F/M) or NFU1 mutants (+NFU1$^{NM\text{-}AA}$-F/M and + NFU1$^{FY\text{-}AA}$-F/M). Lysates from MCH46 and the NFU1 Pt cells transfected with the empty vector (+pCMV6-F/M) were used as positive and negative controls, respectively. As observed in Figure 7A, a decrease in the LIAS activity reflected by diminished lipoylated pyruvate dehydrogenase complex (LA-PDH) and lipoylated α-ketoglutarate dehydrogenase (LA-KGDH) in the NFU1 Pt cells was partially restored by the complementation with the WT-NFU1 but not upon complementation with NFU1$^{FY\text{-}AA}$ or NFU1$^{NM\text{-}AA}$ (Fig. 7A) and a subtle but similar trend was observed in the protein levels of SDHB. Protein levels of another [4Fe–4S] cluster containing enzyme, ACO2, did not change, and SDHA (which functions in close association with SDHB) protein levels were stable, whereas levels of the extra-mitochondrial [4Fe–4S] cluster protein ABCE1 increased in the NFU1 Pt cells as compared to the WT, for unknown reasons (Fig. 7A). Interestingly, the protein levels of both ISCU and ISCA1 were consistently upregulated in the NFU1 Pt cells, suggesting that an uncharacterized mechanism of regulating in the ISC biogenesis pathway was induced to increase expression of donor Fe–S proteins to compensate for the loss of functional NFU1 (Fig. 7A). We also assessed the activities of respiratory complexes (CI and CII) by the in-gel activity assay. While CI seemed to be more adversely affected than CII in the NFU1 Pt cells, the activities of both complexes were only marginally restored by complementation with WT-NFU1 (Fig. 7B). The fact that the complementation of the Pt cells with WT-NFU1 restored lipoylation more efficiently than the activities of CI and CII at the time of analysis post-complementation suggests that NFU1 may be directly involved in cluster transfer to LIAS, but perhaps indirectly involved in cluster transfer to the CI or CII subunits. The differences in the degree of complementation can be partially attributed to direct versus indirect effects due to loss of functional NFU1 on CI and CII activities, as well as to the fact that the complementation assays were performed by transiently transfecting WT-NFU1 in the patient cells. Taken together, these results indicate that the association and dissociation of NFU1 with its Fe-S cluster donor proteins mediated by FY and NM residues, respectively, were critical for the physiological role of NFU1, i.e., to deliver the Fe-S clusters to its target proteins.

ISCA1 functioned upstream of NFU1 and responded to the loss of function of NFU1 *in vivo*

To address if ISCA1 functioned upstream of NFU1 as an Fe–S cluster donor, we studied the biochemical effects elicited by silencing ISCA1 in WT and NFU1 Pt cells. An effective knockdown of ISCA1

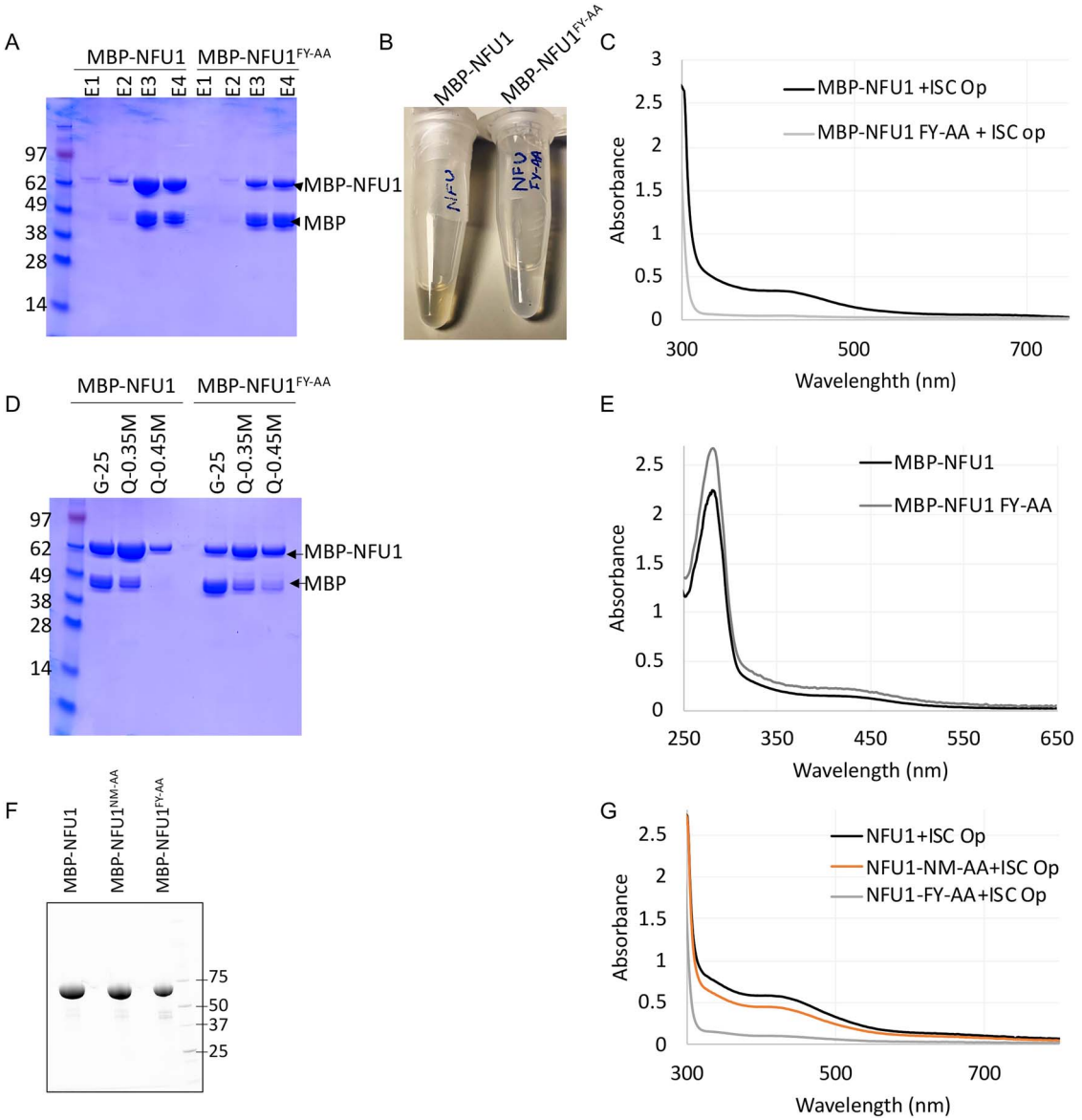

Figure 6. NFU1^{FY-AA} mutant cannot acquire an Fe–S cluster *in vivo*, but the NFU1^{FY-AA} mutant can acquire the Fe–S cluster upon *in vitro* chemical reconstitution. (**A**) Coomassie-stained SDS gel of the eluates (E1, E2, E3, E4) obtained upon affinity purification by amylose resin of MBP-NFU1 (WT) and MBP-NFU1^{FY-AA} proteins. (**B**) E3-MBP-NFU1 solution was brown in color, whereas E3- MBP-NFU1^{FY-AA} was not. (**C**) UV–visible spectra of anaerobically purified (E3) MBP-NFU1 (WT) and (E3) MBP-NFU1^{FY-AA} from *E. coli* co-expressing the ISC operon from *A. vinelandii*. (**D**) Coomassie-stained SDS gel of the chemically reconstituted purified proteins obtained from the desalting column (G-25) and the HiTrap Q column at 0.35 and 0.45 M NaCl concentration. (**E**) UV–visible spectra of anaerobically reconstituted and HiTrap Q column purified MBP-NFU1 (WT) and MBP-NFU1^{FY-AA} at 0.35 M NaCl concentration. (**F**) Stain-free SDS PAGE separation and (**G**) UV–visible spectra of as-purified MBP-NFU1 (WT) and MBP-NFU1^{FY-AA} and MBP-NFU1^{NM-AA} proteins.

was achieved by performing two rounds of siRNA transfections over 6 days. As previously reported (21), the levels of both NFU1 and ISCU did not seem to be significantly affected by the loss of ISCA1 (Fig. 8A). Conversely, the loss of NFU1 in Pt cells correlated with increased levels of ISCU and ISCA1 (Fig. 8A). Furthermore, we observed that loss of either NFU1 or ISCA1 caused a decrease in protein levels of LA-PDH and LA-KGDH, which was much more pronounced when both ISCA1 and NFU1 were simultaneously decreased through silencing of ISCA1 in NFU1 Pt cells (Fig. 8A). The profound loss in the activity of LIAS caused by simultaneous loss of functional NFU1 and ISCA1 suggested that ISCA1 was involved in the process of lipoylation, independent of NFU1. Furthermore, a profound loss of SDHB protein levels upon the knockdown of ISCA1 but a marginal decrease in the NFU1 Pt cells suggested that the two proteins are engaged in different Fe–S cluster delivery pathways. Thus, based on these results, LIAS appeared to be a clear primary target of NFU1. Taken together, these results indicate that ISCA1 functioned as an upstream Fe–S cluster donor that donated its cluster to other mitochondrial targets in addition to

While NFU1 in humans is an indispensable protein, in other organisms such as yeast and bacteria, its orthologs are dispensable but are induced under oxidative stress conditions (24,25,42,47). To determine if NFU1 expression was regulated by oxygen concentration in human cells, we grew the NFU1-Pt and WT fibroblasts under atmospheric oxygen as well as hypoxia conditions (2.5% O_2) and measured the transcript levels of *NFU1*, *ISCU* and *ISCA1* in these cells. The transcript levels of *NFU1* were

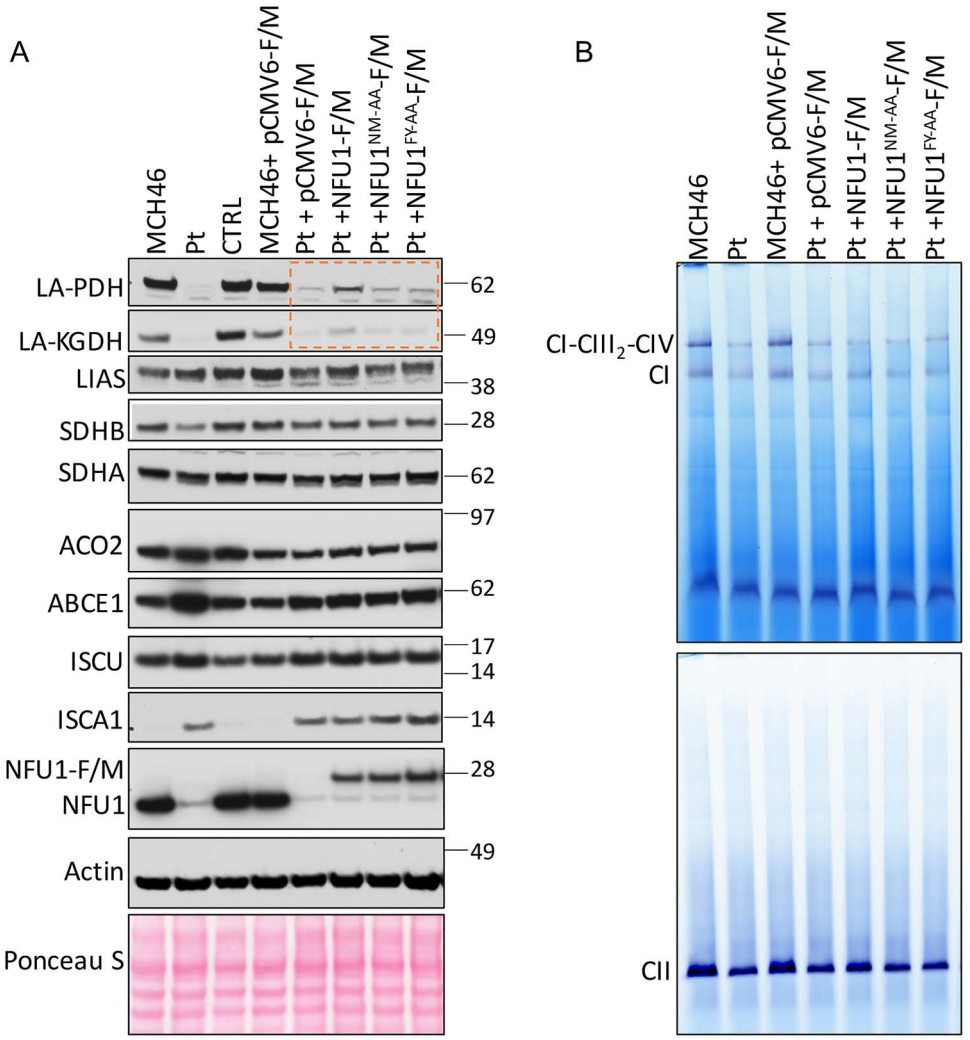

Figure 7. Biochemical deficiencies in NFU1^{R182Q} patient-derived fibroblasts can be partially rescued by WT-NFU1 but not by NFU1^{N226A_M227A} or NFU1^{F230A_Y231A}. (**A**) Immunoblots on total cell lysate were performed with antibodies to the proteins labeled on the vertical axis, and (**B**) in-gel assay for CI and CII on the mitochondrial extracts of MCH46, CTRL and NFU1^{R182Q} patient (Pt) fibroblast mitochondrial lysates complemented with constructs expressing WT-NFU1-F/M, NFU1^{N226A_M227A}-F/M, NFU1^{F230A_Y231A}-F/M, NFU1^{C210A_C213A}-F/M or the empty vector pCMV6-F/M. Rescue of lipoylation by transfection with NFU1-F/M, but not by NFU1^{FY-AA}-F/M or NFU1^{NM-AA}-F/M mutants, is highlighted by the orange box in A.

reduced in the patient cells as expected (30), but irrespective of the oxygen levels, the transcripts of both *ISCU* and *ISCA1* were significantly upregulated compared to WT in the NFU1 Pt cells, suggesting that cells have a mechanism to transcriptionally respond to loss of functional NFU1 at all times (Fig. 8B–D). Nevertheless, the presence of small but detectable transcripts in the WT and upregulated *ISCU* and *ISCA1* transcripts in NFU1 Pt cells under hypoxic conditions points towards the indispensable nature of NFU1 in humans.

Identification and characterization of new pathogenic mutations in NFU1

Upon the discovery of the significance of the NM and FY residues of NFU1 for Fe–S cluster acquisition and delivery, we inspected the SNP databases to identify human variants with mutations in the region of interest. In our search, we found three variants available (N226D, M227I and Y231C) on the NCBI SNP database, one of which (N226D) was annotated as likely pathogenic. To functionally characterize these variants, we generated NFU1-F/M mutants corresponding to NFU1^{N226D}-F/M, NFU1^{M227I}-F/M and NFU1^{Y231C}-F/M. We analyzed the interaction of these mutants with ISCU2 and ISCA1 as well as their ability to complement the loss of NFU1 in the NFU1 Pt cells. While all three variants showed marginal reduction in the interaction with ISCA1 (Fig. 9A), NFU1^{N226D}-F/M showed increased binding with ISCU2 (Fig. 9B). Phenotypically, NFU1^{N226D}-F/M showed impaired ability to complement the loss of NFU1 as demonstrated by its inability to restore lipoylation of PDH and KGDH or to restore SDHB protein levels (Fig. 9C). Complementation by NFU1^{M227I}-F/M and NFU1^{Y231C}-F/M was also compromised. Thus, these results revealed new mutations in human NFU1, which exhibited pathogenicity due to their inability to effectively acquire and subsequently deliver the Fe–S cluster to the target proteins (LIAS and SDHB).

Discussion

The significance of Fe–S clusters in cellular metabolism and their association with the etiologies of several rare diseases

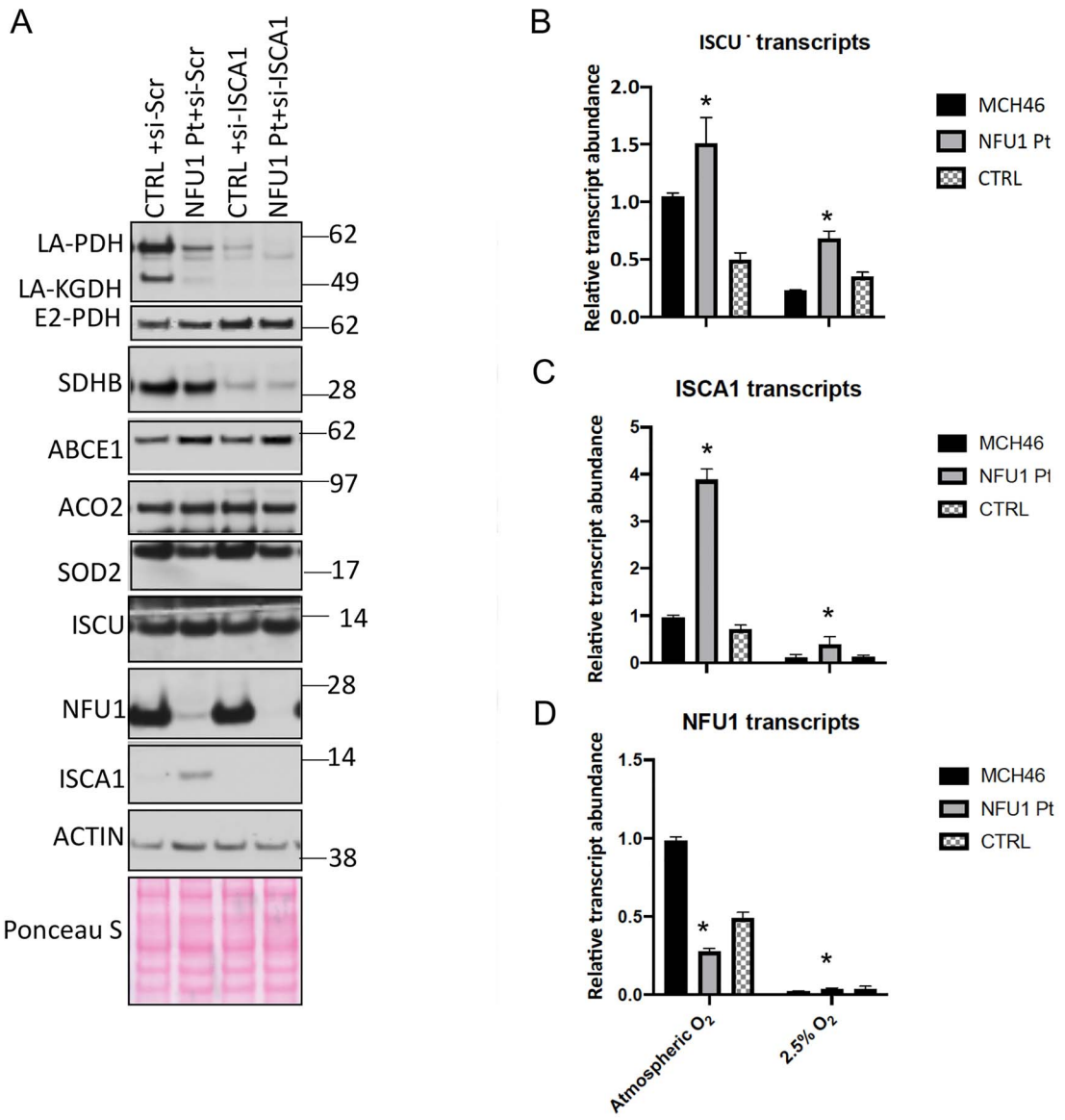

Figure 8. ISCA1 is required for NFU1-mediated lipoylation and SDHB stabilization in human cells. (**A**) NFU1 and ISCA1 independently affected Fe–S cluster proteins in human cells. Control (CTRL) and NFU1^{R182Q} patient (Pt) fibroblasts were transfected twice for 6 days with siRNAs targeting ISCA1 (si-ISCA1) or non-specific scramble si-RNAs (si-Scr). Immunoblots of total cell lysate demonstrate the effects on various proteins involved in Fe–S cluster pathway. (**B–D**) Relative expression levels of (B) *ISCU*, (C) *ISCA1* and (D) *NFU1* transcripts were measured by quantitative real-time polymerase chain reaction on the control (MCH46 and CTRL) and NFU1^{R182Q} patient (NFU1-Pt) fibroblasts grown in 21% (atmospheric oxygen) or at 2.5% oxygen (hypoxia) conditions. Transcript levels were normalized to β-actin. Asterisks (*) represent a significant change in the transcript levels in NFU1 Pt cells relative to the control cells ($P < 0.05$).

has made it essential to have a complete understanding of the mechanisms that govern Fe–S cluster biogenesis and trafficking of the clusters to recipient proteins. *De novo* biosynthesis of Fe–S clusters begins with the assembly of a nascent [2Fe–2S] cluster upon the main scaffold protein ISCU2, which functions as a building block to generate [3Fe–4S] and [4Fe–4S] clusters that are subsequently distributed to recipient Fe–S apo-proteins by additional proteins and complex pathways. The recognition that a tripeptide motif (Leu-Tyr-Arg) in the sequence of SDHB binds the co-chaperone, HSC20, and enables the HSC20/HSPA9 chaperone-co-chaperone complex to transfer the [2Fe–2S] cluster from ISCU to a target protein demonstrated that an energy consuming pathway is employed by cells to specifically transfer Fe–S clusters from the initial biogenesis machinery to recipient proteins (17). Here, we report another pathway that illustrates how [2Fe–2S] cluster building blocks are used in mammalian cells to assemble a [4Fe–4S] cluster, which is eventually transferred to specific recipient proteins. We employed genetic and biochemical techniques to show that the assembly of a [4Fe–4S] cluster on NFU1 requires coordinated interactions with two [2Fe–2S] cluster-containing proteins, the main scaffold ISCU2 and the intermediate carrier ISCA1 *in vivo*. The cluster thus assembled on NFU1 is then directly transferred to its target proteins, such as LIAS. By studying direct protein–protein interactions and performing co-IPs, our study reveals that direct protein interactions are required for the physiologically relevant acquisition and delivery of a [4Fe–4S] cluster from the initial biogenesis proteins to the recipient proteins in cells.

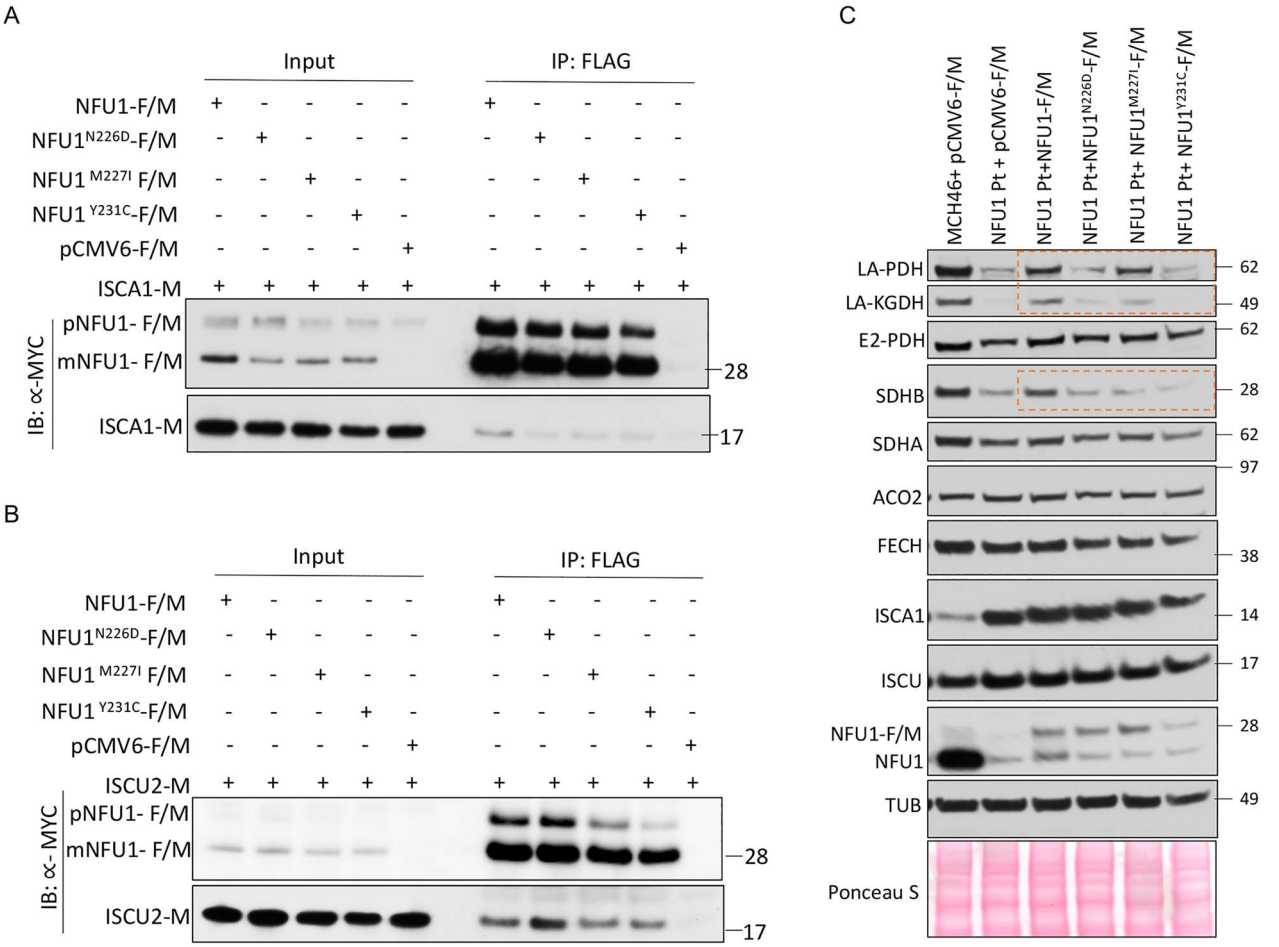

Figure 9. Characterization of natural pathogenic NFU1 mutations. HeLa cell extracts co-transfected with NFU1-F/M or SNP mutants of NFU1-F/M ($NFU1^{N226D}$, $NFU1^{M227I}$, $NFU1^{Y231C}$) or the empty vector (pCMV6-F/M) along with (**A**) ISCA1-M or (**B**) ISCU2-M were immunoprecipitated with anti-FLAG beads (mouse) and immunoblotted with anti-MYC (rabbit) antibody. pNFU1-F/M:FLAG and MYC tagged precursor NFU1, m-NFU1-F/M:FLAG and MYC tagged mature mitochondrial NFU1 isoform. (**C**) Biochemical deficiencies of $NFU1^{R182Q}$ Pt fibroblast were partially rescued by WT-NFU1 (NFU1-F/M) but not by NFU1 SNP mutants as shown by the western blots probing for lipoylated PDH and KGDH as well as SDHB (orange boxes).

An *in vitro* study recently reported that NFU1 acquires its [4Fe–4S] cluster directly from ISCU (22). Notably, that study demonstrated that only ISCU that bound a [4Fe–4S] cluster and not ISCU with a [2Fe–2S] cluster was able to transfer the cluster to NFU1. While the physiological relevance of ISCU ligating a [4Fe–4S] cluster remains controversial (48–50), our study agrees with the observation that ISCU ligating a [2Fe–2S] cluster alone cannot deliver [4Fe–4S] cluster to NFU1. In our experiments, we found that NFU1 engaged directly with two [2Fe–2S] cluster containing proteins, ISCU2 and ISCA1, via a common and conserved hydrophobic motif (F_{230}_Y_{231}; FY) (Figs 1, 2, 4). The initial screening that identified the role of NFU1-FY residues as the binding site for ISCU2 was primarily based on the Y2H assay. Mutagenesis of several residues buried in the core (including I224A, L228A and I231A, V234A) of the CTD-NFU1 protein structure resulted in inconclusive, non-specific growth patterns relative to the negative control (Supplementary Material, Fig. S2D and E), perhaps due to the misfolding of the mutated proteins in yeast (36). Thus, while more residues on NFU1 might play a supporting role in its interactions with ISCU2 and ISCA1 (22), the mutagenesis of FY residues of NFU1 specifically reduced its interaction with either ISCU2 or ISCA1 and suggests that the FY motif is directly involved in the interaction with each of the two scaffold proteins (Figs 2 and 4). The FY motif of NFU1 was also shown to be essential for the biological acquisition of the Fe–S cluster, thereby confirming the roles of the interacting proteins as the physiological Fe–S cluster donors (Fig. 6). Furthermore, the reduced cluster occupancy on NFU1 upon the knockdown of mammalian *ISCA1* or bacterial *IscA* in the ISC operon, as well as the loss of the residues of NFU1 ($N_{226}M_{227}$) that specifically engaged in an interaction with ISCU2, provided direct evidence that supported the role of both ISCA1 and ISCU2 as the Fe–S cluster donors to NFU1 (Figs 5 and 6). Finally, the inability of $NFU1^{FY\text{-}AA}$ and $NFU1^{NM\text{-}AA}$ mutants to restore the biochemical defects of the NFU1 Pt cells in the complementation assays provided strong evidence that both ISCU and ISCA1 were essential to assemble a functional cluster on NFU1 (Fig. 7). These data collectively suggest that ISCU2 and ISCA1 each donate a [2Fe–2S] cluster to the NFU1 dimer, which is then potentially assembled into a [4Fe–4S] cluster by the reductive coupling mediated by FDX2, another direct interacting partner of NFU1 detected in this study.

In our study, we did not detect interactions of NFU1 with other presumed Fe–S scaffolds/donors including ISCA2, IBA57,

GLRX5 or BOLA3. A complex composed of ISCA1–ISCA2–IBA57 has been suggested to function as the intermediate carrier that assembles the [4Fe–4S] cluster for the downstream late-acting carrier proteins including NFU1 and BOLA3 (21,25,51). However while ISCA1 and ISCA2 can interact with each other, the two proteins appear to have distinct binding partners *in vivo*, including IBA57, which was shown to interact only with ISCA2 and to be regulated by the levels of ISCA2 (43,52). Furthermore, only ISCA1, and not ISCA2, was shown to be essential for [4Fe–4S] cluster assembly in skeletal and neuronal tissue under physiological conditions (43). Our work also supports that only ISCA1 and not ISCA2 or IBA57 is essential for the assembly of a [4Fe–4S] cluster on NFU1 (Figs 4 and 5). *In vitro* studies recently showed that a heterotetrameric complex between dimers of GLRX5 and BOLA3 transferred a [4Fe–4S] cluster to NFU1 (20). This pathway may serve as an alternative pathway, given that one patient with GLRX5 mutation was reported to have a NFU1-like phenotype (23). However, patients with NFU1 mutations develop MMDS1, whereas the clinical presentation of two GLRX5-deficient patients was mainly limited to sideroblastic anemia, suggesting that although Fe–S cluster trafficking pathways that involve GLRX5 and NFU1 may partially overlap, the pathway outlined in this article may represent the predominant pathway in most cells (53–55).

While the existence of other pathways to deliver the Fe–S cluster to NFU1 is plausible, the cluster transfer from ISCU2 and ISCA1 mediated by FY motif is physiologically relevant and appears to be absolutely essential for the function of targets such as LIAS (Fig. 7). In this study, we showed that NFU1 interacts directly with two known [4Fe–4S] cluster recipient proteins, SDHB and LIAS *in vivo*, a novel previously unreported observation (Fig. 1). Despite interacting directly with NFU1, SDHB protein levels do not appear to be significantly modulated by the levels of NFU1 (Fig. 7). Further investigations will be required to establish the role of NFU1 in Fe–S cluster delivery from NFU1 to SDHB. In bacteria, the mechanism for the cluster delivery to LIAS was recently elucidated in *E. coli* (47). LipA, the LIAS counterpart in bacteria, ligates two [4Fe–4S] clusters (56). NfuA, the bacterial homologue of NFU1 that is larger (24) and multifunctional, was shown to replenish the rapidly turned over auxiliary cluster in LipA that donates sulfur for lipoic acid formation; however, the source for the stable SAM [4Fe–4S] cluster was not discovered (47). Although this mechanism remains to be investigated in humans, NFU1 may supply the auxiliary Fe–S cluster in LIAS and thereby enable LIAS to maintain its activity. ISCA1, which appears to independently contribute to LIAS activity (Fig. 8), could be involved in the delivery of the SAM cluster in LIAS. According to our data, ISCA1 appears to function as an upstream protein that is involved in donating its cluster to other mitochondrial proteins in addition to NFU1 (Fig. 8). Similarly, SDHB appears to depend on ISCA1 for acquisition of one or more of its cluster(s), which in turn affects its stability in the mammalian cells in which *ISCA1* is silenced (Fig. 8). Further studies are required to establish if an ISCA1 dimer directly donates a [4Fe–4S] cluster to these targets or if it mediates transfer through another terminal donor. Identification of shared sequence features in the binding sites for Fe–S cluster carrier proteins in multiple recipients may help to define a motif that can be used informatically to identify other potential unrecognized [4Fe–4S] cluster containing proteins.

In conclusion, we showed that NFU1 directly interacts with two Fe–S cluster biogenesis proteins (ISCU2 and ISCA1) through its conserved FY motif, and these interactions are required for the physiological acquisition of the cluster by NFU1. The analysis of the multimeric protein complexes containing NFU1 by native/2D SDS-PAGE provided further insights into the mechanism of the assembly of the [4Fe–4S] cluster on NFU1 and its delivery to its target proteins (Fig. 1I). Although the transfer of Fe–S clusters from holo-ISCU (22) and holo-ISCA1 (57) to apo-NFU1 has been previously reported *in vitro*, further investigations are required to establish the sequence of events required for the Fe–S cluster transfer which may reveal alternative pathways under specific conditions. Based on our observations, we postulate that both ISCU2 and ISCA1 interact with the FY motif of NFU1 and donate their respective [2Fe–2S] clusters to NFU1, which coalesce into a [4Fe–4S] cluster upon the donation of electrons by FDX2 (Fig. 10). The fact that both the CXXC and FY motifs are essential for the interaction between NFU1 and ISCA1 (Fig. 4) suggests that NFU1 may acquire its first [2Fe–2S] building block from ISCU2, which may be ligated transiently between ISCU2 and one monomer of NFU1 or between the two monomers of NFU1 via the $C_{210}\_C_{213}$ motif of each monomer. This proposed partial loading may then permit ISCA1 containing the second [2Fe–2S] cluster to be to recruited and bind to NFU1 at its FY motif (Fig. 4). The interaction between ISCA1 and ISCU2 (Figs 1 and 4) may facilitate the recruitment of ISCA1 by NFU1. We envision that the delivery of the second cluster from ISCA1 allows the two [2Fe–2S] clusters to coalesce into a [4Fe–4S] cluster when FDX2 provides a reducing equivalent and enhances the formation of a stable cubane [4Fe–4S] cluster. This assembly complex containing holo-NFU1 may then recruit the apo-target proteins such as LIAS and thus act as a terminal Fe–S cluster donor to recipient proteins (Figs 1I and 10), as was observed in the case of bacterial LipA (58). Finally, the identification and characterization of new NFU1 pathogenic mutations in the human population provide genetic information that may facilitate early diagnosis of MMDS1 (Fig. 9). Thus, our study elucidates a complete pathway employed by mammalian cells that illustrates how basic [2Fe–2S] clusters are converted into [4Fe–4S] clusters on an intermediate scaffold protein, which then conveys its Fe–S cluster to recipient proteins through direct protein-binding interactions.

Materials and Methods

Primary cultures

Two immortalized WT fibroblast cell lines (MCH46 and CTRL), which were used as controls, and $NFU1^{R182Q}$ fibroblasts derived from patients (NFU1 Pt) were previously generated (30). Fibroblasts were cultured in Dulbecco's modified Eagle's medium (DMEM) containing 5 mM glucose and 1 mM sodium pyruvate (Thermo Fisher Scientific) and supplemented with 10% fetal bovine serum (FBS) (CellGro) and 2 mM glutamine. HeLa or HEK293 cells purchased from ATCC were cultured in DMEM supplemented with 10% FBS, 4.5 g/l glucose along with 2 mM glutamine. Cells were grown at 37°C and 5% CO_2 in a humidified incubator at atmospheric oxygen concentration unless mentioned otherwise.

Cloning and plasmid constructs

The plasmids used to transfect human cells were all pCMV6-Entry-based vectors (Origene) to allow the expression of the full-length gene of interest under the CMV promoter (Supplementary Material, Table S1). The constructs were C-terminally tagged with FLAG/MYC. Plasmid transfections into human cells were routinely performed using Lipofectamine 2000 (Thermo Fisher Scientific) according to the manufacturer's

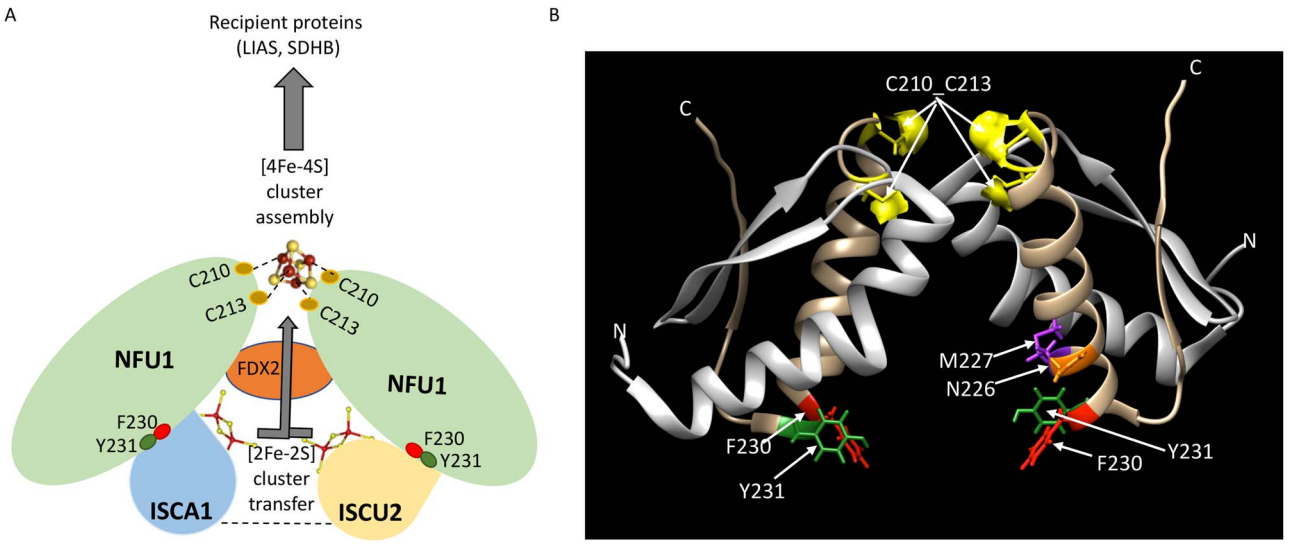

Figure 10. Proposed model for the assembly of a [4Fe–4S] cluster on NFU1. (**A**) Two [2Fe–2S] clusters, each ligated by holo-ISCA1 and holo-ISCU2, are transferred to dimeric NFU1 and assembled into a [4Fe–4S] cluster by a reductive coupling mediated by FDX2. The [4Fe–4S] cluster assembled on NFU1 is subsequently transferred to recipient proteins such as LIAS and SDHB. We postulate that NFU1 initially binds ISCU2 via its F_{230}_Y_{231} residues and transiently ligates the [2Fe–2S] cluster via C_{210}_C_{213}. This partial loading of the cluster on NFU1 via C_{210}_C_{213} is necessary to recruit ISCA1 (mediated by the FY and the CXXC motifs of NFU1) and thereby incorporate the second [2Fe–2S] cluster from ISCA1. This process may be facilitated by the affinity of ISCA1 for binding to ISCU2 (represented by the dashed line between ISCA1 and ISCU2; Figs 1 and 4). The delivery of the second cluster from ISCA1 allows two [2Fe–2S] clusters to coalesce into a single [4Fe–4S] cluster that forms a bridge between the two NFU1 monomers, aided by donation of reducing equivalents from FDX2, which permits the formation of a stable bridging [4Fe–4S] cluster. It is possible that the [2Fe–2S] cluster is transiently ligated between the two NFU1 monomers, which is then converted into a more stable [4Fe–4S] cluster by FDX2 upon the recruitment of ISCA1 and acquisition of its cluster. The assembly complex containing holo-NFU1 subsequently recruits the apo-target proteins such as LIAS (as shown in Fig. 1I) and thus acts as a terminal Fe–S cluster donor to recipient proteins (**B**) The ribbon model representation of a dimer of CTD-NFU1 (PDB:2M5O) displaying the residues involved in the binding of ISCA1 (F230, Y231; left) and ISCU (N226, M227, F230, Y231; right) on each monomer. The [4Fe–4S] is ligated via C210 and C213 between the two NFU1 monomers. Color coding of the residues: NFU1—red, F230; green, Y231; purple, M227; orange, N226; yellow, C210_C213.

instructions. Point mutations/deletions were introduced using QuikChange II XL Site-Directed Mutagenesis Kit (Agilent).

The plasmids, pGADT7 and pGBKT7 (Takara), were used as prey and bait vectors, respectively, for the Y2H screens. The cDNAs encoding ISCU2 and NFU1 were subcloned in the prey vector (pGADT7) and the cDNAs encoding ISCA1, ISCA2, IBA57, FDX2, GLRX5, BOLA3 and NFU1 were subcloned in the bait vector (pGBKT7) from their respective pCMV6 constructs or the HeLa cell cDNA (Supplementary Material, Table S1) using HiFi cloning kit [New England Biolabs (NEB)] according to the manufacturer's instructions. These cDNAs were cloned at the 3′ end of GAL4 activation domain (AD) and the GAL4 DNA binding domain (BD) in the prey and bait vectors, respectively, such that the proteins encoded by these inserts were fused to the C-terminus of either GAL4 AD or BD, which rendered their mitochondrial targeting sequences non-functional. SDHB-prey and LIAS-prey constructs were obtained from the Mate & Plate™ Library (Takara). Rabaptin/RABEP1-prey, SV40 T-antigen-prey, RABEX5-bait and p53-bait were used as controls as previously reported (17). The AD as well as DNA BD of GAL4 contained the nuclear localization signal, which ensured the translocation of each expressed construct into the nucleus upon translation, thereby facilitating possible interactions in the same cellular compartment.

The plasmids used for bacterial overexpression and protein purification encoding NFU1 and ISCA1 were subcloned into pMAL-c5x vector (NEB) expressing maltose binding protein (MBP) at the N-terminus of the fusion construct generating MBP-NFU1 or MBP-ISCA1 using HiFi cloning kit (NEB) following the manufacturer's instructions. pBDR1421 (a kind gift from Dr Caroline Philpott who obtained the operon from Dr Dennis Dean) was used to overexpress the ISC operon (ISC operon encodes: *IscR, IscS, IscU, IscA, hscB, hscA, fdx, iscX*).

The ISC operon deleted for *IscA* (IscA-del-Op) was generated by site-directed mutagenesis (Agilent). To avoid the polar effects on the expression of downstream genes in the operon, an in-frame deletion of *IscA* in the ISC operon was performed by looping out a majority of *IscA* CDS, leaving behind at least 18–21 nucleotides, corresponding to 6–7 amino acids intact on each end of the gene in the ISC operon. In-frame deletions or substitutions generally do not adversely affect the expression of downstream genes (59,60).

SiRNA transfection of human cells

On-TARGETPlus siRNA pools against human *ISCA1* (L-014678-02-0005) and the control non-targeting pool (D-001810-10-05) were purchased from Dharmacon. Knockdown of *ISCA1* was achieved by transfecting cells twice with siRNAs at a 48-h interval using Dharmafect 1 according to manufacturer's instructions.

Y2H assay

150 ng each of the prey and the bait constructs were co-transformed into the AH109 competent cells using the EZ transformation kit following the manufacturer's instructions (MP Biomedical) and plated on leucine and tryptophan drop-out media (-Leu/-Trp) for 4 days. This media provided the selection pressure to select the cells harboring both the bait and prey plasmids, which encoded Leu and Trp biosynthesis genes, respectively, that are otherwise absent from the cell. The interaction of the bait and prey constructs was engineered to activate the transcription of *HIS3* gene, thus allowing the cells to grow in the media devoid of histidine (His). 3-Aminotriazole (3-AT), a competitive inhibitor of HIS3,

was added to the media to neutralize leaky expression of HIS3, thus increasing the stringency of the media for the interaction. To test the interactions between preys and baits, four transformed colonies from each Leu/-Trp plate were pooled and resuspended in ultrapure water. The concentration of the cells in the solution was subsequently normalized to OD = 0.05. 5 µl of the cells were spotted on -Leu/-Trp, -Leu/-Trp/-His, -Leu/-Trp/-His/+ 3-AT with increasing 3-AT concentrations as indicated along the individual figures. The growth of the cells was monitored over 5 days. Two pairs of known interacting proteins, Rabaptin-Rabex and SV40 Tag-p53, were used as controls.

IP in transfected mammalian cells

12 µg of NFU1-FLAG/MYC (NFU1-F/M) along with 10 µg ISCU2-MYC (ISCU2-M) or 10 µg ISCA1-MYC (ISCA1-M) were co-expressed in HeLa cells (ATCC). Twenty-four hours post transfection, cells were harvested in a lysis buffer (25 mM Tris, 0.15 mM NaCl, 1 mM EDTA, 1% NP-40, 5% glycerol, protease inhibitor cocktail, pH 7.4) and 750 µg of the total proteins were incubated overnight at 4°C with either EZ View Red Anti-Flag Beads (Sigma) or beads chemically crosslinked with anti-ISCU (Origene), anti-ISCA1 (Sigma) or anti-NFU1 antibodies. The beads were subsequently harvested by centrifugation, washed in the lysis buffer followed by Dulbecco's phosphate-buffered saline (DPBS) washes and finally boiled to elute the proteins bound to the beads. Five percent of the post-transfection lysates were loaded as inputs for the respective samples and ~17% of the eluted samples were loaded in the IP lanes per sample. Immunoblots (IBs) were performed with antibodies as indicated on the figure panels and in Supplementary Material, Table S2.

Protein purification and Fe–S cluster reconstitution

Recombinant pMAL-c5X vector was co-expressed with ISC operon-pBDR1421 in BL(DE)21 bacteria. The pre-inoculum was used to grow a 250 ml culture expressing MBP-NFU1 or MBP-ISCA1 with the ISC operon vector. The ISC operon was induced with 0.2% D-arabinose at the OD = 0.3 and then with 0.3 mM IPTG at OD = 0.6. The culture was supplemented with 0.1 mM L-cysteine and 25 µM ferric ammonium citrate (58) and grown with shaking at 140 rpm at 15°C overnight. Cells were pelleted by centrifugation at 4°C at 5000*g*. The cell pellet was lysed with 1× BugBuster™ (ENDMillipore) in PBS for 30 min at 4°C and then centrifuged at 16 000*g* for 25 min to extract the soluble protein lysate. The soluble lysate was incubated with 1 ml amylose beads (NEB) anaerobically (batch purification) overnight and subsequently washed and eluted with 10 mM maltose. For further purification, the buffer of the eluted protein was exchanged to 50 mM HEPES, pH 6.2 using PD-10 column (Sigma), and the eluted protein was then further purified using a HiTrap Q column (Sigma) from which the purified protein was subsequently eluted by stepwise increasing NaCl concentrations. NFU1 was eluted at 0.3–0.35 M NaCl, 50 mM HEPES. ISCA1 was eluted at 0.15–0.2 M NaCl. 100 µM purified protein was anaerobically reconstituted with Fe–S cluster as described (20,58). All the buffers contained 5 mM DTT and 10% glycerol (58). The purified protein was then visualized on the stain-free SDS gel or Coomassie-stained SDS gel; the UV–visible spectrum was recorded using Nanodrop OneC (Thermo Fisher Scientific).

Iron incorporation assay

The ^{55}Fe incorporation assay was performed essentially as previously described (17,19), with minor modifications. HEK293 cells were grown in the presence of 1 µM ^{55}Fe-Tf for the duration of the experiment and transfected twice at 48-h interval with siRNAs targeting *ISCA1* or with non-targeting siRNAs, as indicated. At the time of the second transfection with siRNAs, cells were co-transfected with FLAG/MYC-tagged NFU1 or with the empty vector (pCMV6-Entry; Origene CAT#: PS100001), which was used to normalize the results. Mitochondrial extracts were prepared as previously described (17) and subjected to immunoprecipitation with anti-FLAG M2 agarose beads to immunocapture recombinant NFU1-F/M.

^{55}Fe incorporation into recombinant FLAG-MYC-tagged NFU1 was measured by scintillation counting of FLAG-beads after immunoabsorption of FLAG-tagged recombinant NFU1-F/M, followed by extensive washing with buffer I (25 mM Tris, 0.15 M NaCl, 1 mM EDTA, 1% NP-40, 5% glycerol (pH 7.4), protease and phosphatase inhibitor cocktail with no EDTA (Roche)). The background, corresponding to ^{55}Fe measurements of eluates after anti-FLAG immunoprecipitations on mitochondrial extracts from cells transfected with the empty vector, was subtracted from each reading. Unpaired *t*-test analyses of ^{55}Fe labeling experiments were performed with GraphPad Prism 7.

ISCA1 knockdown and complementation analysis of NFU1^{R182Q} patient (NFU1 Pt) fibroblasts

ISCA1 knockdown was performed by transfecting control (CTRL) or NFU1 Pt cells with si-ISCA1 (Dharmacon) according to the manufacturer's instructions. Si-SCR (non-targeting pool of siRNAs; Dharmacon) were used as controls. Cells were transfected twice over 6 days to achieve an efficient knockdown. For complementation studies, MCH46 and NFU1 Pt fibroblasts (30) were transfected with either pCMV6-F/M or pCMV6-NFU1-F/M (WT or mutants, as indicated) for 60 h in serum-free media using Lipofectamine 2000 according to the manufacturer's instruction. Total lysates were prepared in lysis buffer (25 mM Tris, 0.15 mM NaCl, 1 mM EDTA, 1% NP-40, 5% glycerol, protease inhibitor cocktail, pH 7.4) and 30–40 µg total proteins were loaded per lane on SDS-PAGE (Thermo Fisher Scientific) and probed with the different antibodies, as indicated (Supplementary Material, Table S2). The CI and CII in-gel activity assays were performed on the mitochondrial extracts of the aforementioned fibroblasts as previously reported (17).

Quantitative real-time polymerase chain reaction

Fibroblasts cultured at 21% O_2 or in a hypoxic chamber (2.5%) for 1 week were used to isolate RNA using Qiagen RNeasy kit according to the manufacturer's instructions (Qiagen). 2 µg of RNA was used to prepare cDNA using Applied Biosystems High Capacity cDNA Reverse transcription kit (Fisher Scientific) and the real-time transcript levels of *NFU1*, *ISCU2* and *ISCA1* relative to β-actin were measured and analyzed using Fast SYBR Green Master mix according to the manufacturer's instructions (Applied Biosystems).

IP of NFU1-F for native/2D SDS PAGE

Mitochondrial fractions were prepared from HEK293 cells transfected with FLAG-tagged NFU1 (NFU1-F) as previously described (17). IP of NFU1-F was performed using M2-FLAG beads (Sigma). Washed FLAG M2 beads were added to mitochondrial lysates and

incubated for 2 h at room temperature. Beads were recovered after extensive washing, and proteins were competitively eluted with 100 µg/ml 3xFLAG peptide (Sigma).

Two-dimensional native/SDS-PAGE

Two-dimensional native/SDS-PAGE was performed by resolving the eluates after competitive elution of NFU1-F from M2 agarose beads in the first dimension, by BN-PAGE. The NativePAGE Novex Bis-Tris gel system (Thermo Fisher Scientific) was used, with the following modifications: only the light blue cathode buffer was used; the electrophoresis was performed at 150 V for 1 h and 250 V for 2 h. Each lane of the native gel was excised, equilibrated in SDS buffer supplemented with reducing agent and then immersed in the alkylating solution for 15 min, before quenching for an additional 15 min. For the second dimension, the gel strip was fixed horizontally onto the NuPAGE 4–12% Bis-Tris Zoom Gel (Thermo Fisher Scientific), and classical SDS immunoblots were performed.

Supplementary Material

Supplementary Material is available at *HMG* online.

Acknowledgements

We thank Dr Caroline Philpott for pBDR1421 construct and colleagues in the Rouault laboratory for helpful discussions.

Funding

This work was supported by the intramural funding ZIAHD008814 for Mammalian iron-sulfur cluster biogenesis from the National Institutes of Child Health and Human Development and National Institutes of Health.

Conflict of Interest statement. The authors declare no conflict of interest.

Authors' Contributions

A.J. and T.A.R. designed the study and wrote the manuscript. A.J., A.S. and N.M. performed the experiments and analyzed the data. A.J. generated the clones and performed most of the experiments. A.S. performed the co-IP experiments in HeLa cells. N.M. performed the co-IP experiments in HEK293 cells, the 2D-native/SDS-PAGE, ^{55}Fe-incorporation assay and the activity assays of the respiratory complexes in mammalian cells; intellectually contributed to the study and edited the manuscript. T.A.R. analyzed the data and supervised the study. All the authors reviewed the final manuscript.

References

1. Maio, N., Jain, A. and Rouault, T.A. (2020) Mammalian iron–sulfur cluster biogenesis: recent insights into the roles of frataxin, acyl carrier protein and ATPase-mediated transfer to recipient proteins. *Curr. Opin. Chem. Biol.*, **55**, 34–44.
2. Kim, K.S., Maio, N., Singh, A. and Rouault, T.A. (2018) Cytosolic HSC20 integrates de novo iron–sulfur cluster biogenesis with the CIAO1-mediated transfer to recipients. *Hum. Mol. Genet.*, **27**, 837–852.
3. Tong, W.H. and Rouault, T.A. (2006) Functions of mitochondrial ISCU and cytosolic ISCU in mammalian iron–sulfur cluster biogenesis and iron homeostasis. *Cell Metab.*, **3**, 199–210.
4. Adam, A.C., Bornhövd, C., Prokisch, H., Neupert, W. and Hell, K. (2006) The Nfs1 interacting protein Isd11 has an essential role in Fe/S cluster biogenesis in mitochondria. *EMBO J.*, **25**, 174–183.
5. Cory, S.A., Van Vranken, J.G., Brignole, E.J., Patra, S., Winge, D.R., Drennan, C.L., Rutter, J. and Barondeau, D.P. (2017) Structure of human Fe–S assembly subcomplex reveals unexpected cysteine desulfurase architecture and acyl-ACP-ISD11 interactions. *Proc. Natl. Acad. Sci. USA.*, **114**, e5325–e5334.
6. Van Vranken, J.G., Jeong, M.Y., Wei, P., Chen, Y.C., Gygi, S.P., Winge, D.R. and Rutter, J. (2016) The mitochondrial acyl carrier protein (ACP) coordinates mitochondrial fatty acid synthesis with iron sulfur cluster biogenesis. *Elife*, **5**:e17828.
7. Wiedemann, N., Urzica, E., Guiard, B., Müller, H., Lohaus, C., Meyer, H.E., Ryan, M.T., Meisinger, C., Mühlenhoff, U., Lill, R. and Pfanner, N. (2006) Essential role of Isd11 in mitochondrial iron–sulfur cluster synthesis on Isu scaffold proteins. *EMBO J.*, **25**, 184–195.
8. Fox, N.G., Yu, X., Feng, X., Bailey, H.J., Martelli, A., Nabhan, J.F., Strain-Damerell, C., Bulawa, C., Yue, W.W. and Han, S. (2019) Structure of the human frataxin-bound iron–sulfur cluster assembly complex provides insight into its activation mechanism. *Nat. Commun.*, **10**, 2210.
9. Cai, K., Tonelli, M., Frederick, R.O. and Markley, J.L. (2017) Human mitochondrial ferredoxin 1 (FDX1) and ferredoxin 2 (FDX2) both bind cysteine desulfurase and donate electrons for iron–sulfur cluster biosynthesis. *Biochemistry*, **56**, 487–499.
10. Gervason, S., Larkem, D., Mansour, A.B., Botzanowski, T., Muller, C.S., Pecqueur, L., Le Pavec, G., Delaunay-Moisan, A., Brun, O., Agramunt, J. *et al.* (2019) Physiologically relevant reconstitution of iron–sulfur cluster biosynthesis uncovers persulfide-processing functions of ferredoxin-2 and frataxin. *Nat. Commun.*, **10**, 3566.
11. Shi, Y., Ghosh, M., Kovtunovych, G., Crooks, D.R. and Rouault, T.A. (2012) Both human ferredoxins 1 and 2 and ferredoxin reductase are important for iron–sulfur cluster biogenesis. *Biochim. Biophys. Acta*, **1823**, 484–492.
12. Maio, N. and Rouault, T.A. (2015) Iron–sulfur cluster biogenesis in mammalian cells: new insights into the molecular mechanisms of cluster delivery. *BBA–Mol. Cell Res.*, **1853**, 1493–1512.
13. Majewska, J., Ciesielski, S.J., Schilke, B., Kominek, J., Blenska, A., Delewski, W., Song, J.Y., Marszalek, J., Craig, E.A. and Dutkiewicz, R. (2013) Binding of the chaperone Jac1 protein and cysteine desulfurase Nfs1 to the iron–sulfur cluster scaffold Isu protein is mutually exclusive. *J. Biol. Chem.*, **288**, 29134–29142.
14. Vickery, L.E. and Cupp-Vickery, J.R. (2007) Molecular chaperones HscA/Ssq1 and HscB/Jac1 and their roles in iron–sulfur protein maturation. *Crit. Rev. Biochem. Mol. Biol.*, **42**, 95–111.
15. Rouault, T.A. (2012) Biogenesis of iron–sulfur clusters in mammalian cells: new insights and relevance to human disease. *Dis. Model. Mech.*, **5**, 155–164.
16. Braymer, J.J. and Lill, R. (2017) Iron–sulfur cluster biogenesis and trafficking in mitochondria. *J. Biol. Chem.*, **292**, 12754–12763.
17. Maio, N., Singh, A., Uhrigshardt, H., Saxena, N., Tong, W.-H. and Rouault, T.A. (2014) Cochaperone binding to LYR motifs confers specificity of iron sulfur cluster delivery. *Cell Metab.*, **19**, 445–457.

18. Maio, N., Ghezzi, D., Verrigni, D., Rizza, T., Bertini, E., Martinelli, D., Zeviani, M., Singh, A., Carrozzo, R. and Rouault, T.A. (2016) Disease-causing SDHAF1 mutations impair transfer of Fe–S clusters to SDHB. *Cell Metab.*, **23**, 292–302.
19. Maio, N., Kim, K.S., Singh, A. and Rouault, T.A. (2017) A single adaptable cochaperone-scaffold complex delivers nascent iron–sulfur clusters to mammalian respiratory chain complexes I–III. *Cell Metab.*, **25**, 945–953.e946.
20. Nasta, V., Suraci, D., Gourdoupis, S., Ciofi-Baffoni, S. and Banci, L. (2020) A pathway for assembling [4Fe–4S]2+ clusters in mitochondrial iron–sulfur protein biogenesis. *FEBS J.*, **287**, 2312–2327.
21. Sheftel, A.D., Wilbrecht, C., Stehling, O., Niggemeyer, B., Elsasser, H.P., Muhlenhoff, U. and Lill, R. (2012) The human mitochondrial ISCA1, ISCA2, and IBA57 proteins are required for [4Fe–4S] protein maturation. *Mol. Biol. Cell*, **23**, 1157–1166.
22. Cai, K., Frederick, R.O. and Markley, J.L. (2020) ISCU interacts with NFU1, and ISCU[4Fe–4S] transfers its Fe–S cluster to NFU1 leading to the production of holo-NFU1. *J. Struct. Biol.*, **210**, 107491.
23. Baker, P.R., 2nd, Friederich, M.W., Swanson, M.A., Shaikh, T., Bhattacharya, K., Scharer, G.H., Aicher, J., Creadon-Swindell, G., Geiger, E., MacLean, K.N. *et al.* (2014) Variant non ketotic hyperglycinemia is caused by mutations in LIAS, BOLA3 and the novel gene GLRX5. *Brain J. Neurol.*, **137**, 366–379.
24. Bandyopadhyay, S., Naik, S.G., O'Carroll, I.P., Huynh, B.H., Dean, D.R., Johnson, M.K. and Dos Santos, P.C. (2008) A proposed role for the *Azotobacter vinelandii* NfuA protein as an intermediate iron–sulfur cluster carrier. *J. Biol. Chem.*, **283**, 14092–14099.
25. Melber, A., Na, U., Vashisht, A., Weiler, B.D., Lill, R., Wohlschlegel, J.A. and Winge, D.R. (2016) Role of Nfu1 and Bol3 in iron–sulfur cluster transfer to mitochondrial clients. *Elife*, **5**, e15991.
26. Cai, K., Liu, G., Frederick, R.O., Xiao, R., Montelione, G.T. and Markley, J.L. (2016) Structural/functional properties of human NFU1, an intermediate [4Fe–4S] carrier in human mitochondrial iron–sulfur cluster biogenesis. *Structure*, **24**, 2080–2091.
27. Nasta, V., Suraci, D., Gourdoupis, S., Ciofi-Baffoni, S. and Banci, L. (2019) A pathway for assembling [4Fe–4S](2+) clusters in mitochondrial iron–sulfur protein biogenesis. *FEBS J.* **287**, 2312–2327.
28. Tong, W.-H., Jameson, G.N.L., Huynh, B.H. and Rouault, T.A. (2003) Subcellular compartmentalization of human Nfu, an iron–sulfur cluster scaffold protein, and its ability to assemble a [4Fe–4S] cluster. *Proc. Natl. Acad. Sci.*, **100**, 9762–9767.
29. Ahting, U., Mayr, J.A., Vanlander, A.V., Hardy, S.A., Santra, S., Makowski, C., Alston, C.L., Zimmermann, F.A., Abela, L., Plecko, B. *et al.* (2015) Clinical, biochemical, and genetic spectrum of seven patients with NFU1 deficiency. *Front. Genet.*, **6**, 123–123.
30. Cameron, J.M., Janer, A., Levandovskiy, V., Mackay, N., Rouault, T.A., Tong, W.H., Ogilvie, I., Shoubridge, E.A. and Robinson, B.H. (2011) Mutations in iron–sulfur cluster scaffold genes NFU1 and BOLA3 cause a fatal deficiency of multiple respiratory chain and 2-oxoacid dehydrogenase enzymes. *Am. J. Hum. Genet.*, **89**, 486–495.
31. Navarro-Sastre, A., Tort, F., Stehling, O., Uzarska, M.A., Arranz, J.A., Del Toro, M., Labayru, M.T., Landa, J., Font, A., Garcia-Villoria, J. *et al.* (2011) A fatal mitochondrial disease is associated with defective NFU1 function in the maturation of a subset of mitochondrial Fe–S proteins. *Am. J. Hum. Genet.*, **89**, 656–667.
32. Wachnowsky, C., Wesley, N.A., Fidai, I. and Cowan, J.A. (2017) Understanding the molecular basis of multiple mitochondrial dysfunctions syndrome 1 (MMDS1)-impact of a disease-causing Gly208Cys substitution on structure and activity of NFU1 in the Fe/S cluster biosynthetic pathway. *J. Mol. Biol.*, **429**, 790–807.
33. Invernizzi, F., Ardissone, A., Lamantea, E., Garavaglia, B., Zeviani, M., Farina, L., Ghezzi, D. and Moroni, I. (2014) Cavitating leukoencephalopathy with multiple mitochondrial dysfunction syndrome and NFU1 mutations. *Front. Genet.*, **5**.
34. Niihori, M., Eccles, C.A., Kurdyukov, S., Zemskova, M., Varghese, M.V., Stepanova, A.A., Galkin, A., Rafikov, R. and Rafikova, O. (2019) Rats with human mutation of NFU1 develop pulmonary hypertension. *Am. J. Respir. Cell Mol. Biol.*.
35. Rouault, T.A. (2014) Mammalian iron-sulphur proteins: novel insights into biogenesis and function. *Nat. Rev. Mol. Cell Biol.*, **16**, 45–55.
36. Brückner, A., Polge, C., Lentze, N., Auerbach, D. and Schlattner, U. (2009) Yeast two-hybrid, a powerful tool for systems biology. *Int. J. Mol. Sci.*, **10**, 2763–2788.
37. Arcinas, A.J., Maiocco, S.J., Elliott, S.J., Silakov, A. and Booker, S.J. (2019) Ferredoxins as interchangeable redox components in support of MiaB, a radical S-adenosylmethionine methylthiotransferase. *Protein Sci.*, **28**, 267–282.
38. Dong, G., Cao, L. and Ryde, U. (2018) Insight into the reaction mechanism of lipoyl synthase: a QM/MM study. *JBIC Journal of Biological Inorganic Chemistry*, **23**, 221–229.
39. Harmer, J.E., Hiscox, M.J., Dinis, P.C., Fox, S.J., Iliopoulos, A., Hussey, J.E., Sandy, J., Van Beek, F.T., Essex, J.W. and Roach, P.L. (2014) Structures of lipoyl synthase reveal a compact active site for controlling sequential sulfur insertion reactions. *Biochem. J.*, **464**, 123–133.
40. McLaughlin, M.I., Lanz, N.D., Goldman, P.J., Lee, K.-H., Booker, S.J. and Drennan, C.L. (2016) Crystallographic snapshots of sulfur insertion by lipoyl synthase. *Proc. Natl. Acad. Sci.*, **113**, 9446.
41. McCarthy, E.L., Rankin, A.N., Dill, Z.R. and Booker, S.J. (2019) The A-type domain in *Escherichia coli* NfuA is required for regenerating the auxiliary [4Fe–4S] cluster in *Escherichia coli* lipoyl synthase. *J. Biol. Chem.*, **294**, 1609–1617.
42. Py, B., Gerez, C., Huguenot, A., Vidaud, C., Fontecave, M., Ollagnier de Choudens, S. and Barras, F. (2018) The ErpA/NfuA complex builds an oxidation-resistant Fe–S cluster delivery pathway. *J. Biol. Chem.*, **293**, 7689–7702.
43. Beilschmidt, L.K., Ollagnier de Choudens, S., Fournier, M., Sanakis, I., Hograindleur, M.-A., Clémancey, M., Blondin, G., Schmucker, S., Eisenmann, A., Weiss, A. *et al.* (2017) ISCA1 is essential for mitochondrial Fe4S4 biogenesis in vivo. *Nat. Commun.*, **8**, 15124.
44. Ayala-Castro, C., Saini, A. and Outten, F.W. (2008) Fe–S cluster assembly pathways in bacteria. *Microbiol. Mol. Biol. Rev.*, **72**, 110–125.
45. Nordin, A., Larsson, E., Thornell, L.-E. and Holmberg, M. (2011) Tissue-specific splicing of ISCU results in a skeletal muscle phenotype in myopathy with lactic acidosis, while complete loss of ISCU results in early embryonic death in mice. *Hum. Genet.*, **129**, 371–378.
46. Vanlander, A.V. and Van Coster, R. (2018) Clinical and genetic aspects of defects in the mitochondrial iron–sulfur cluster synthesis pathway. *JBIC Journal of Biological Inorganic Chemistry*, **23**, 495–506.

47. McCarthy, E.L. and Booker, S.J. (2017) Destruction and reformation of an iron–sulfur cluster during catalysis by lipoyl synthase. *Science*, **358**, 373.
48. Fox, N.G., Chakrabarti, M., McCormick, S.P., Lindahl, P.A. and Barondeau, D.P. (2015) The human iron–sulfur assembly complex catalyzes the synthesis of [2Fe–2S] clusters on ISCU2 that can be transferred to acceptor molecules. *Biochemistry*, **54**, 3871–3879.
49. Webert, H., Freibert, S.A., Gallo, A., Heidenreich, T., Linne, U., Amlacher, S., Hurt, E., Muhlenhoff, U., Banci, L. and Lill, R. (2014) Functional reconstitution of mitochondrial Fe/S cluster synthesis on Isu1 reveals the involvement of ferredoxin. *Nat. Commun.*, **5**, 5013.
50. Chandramouli, K., Unciuleac, M.C., Naik, S., Dean, D.R., Huynh, B.H. and Johnson, M.K. (2007) Formation and properties of [4Fe–4S] clusters on the IscU scaffold protein. *Biochemistry*, **46**, 6804–6811.
51. Muhlenhoff, U., Richter, N., Pines, O., Pierik, A.J. and Lill, R. (2011) Specialized function of yeast Isa1 and Isa2 proteins in the maturation of mitochondrial [4Fe–4S] proteins. *J. Biol. Chem.*, **286**, 41205–41216.
52. Nasta, V., Da Vela, S., Gourdoupis, S., Ciofi-Baffoni, S., Svergun, D.I. and Banci, L. (2019) Structural properties of [2Fe–2S] ISCA2-IBA57: a complex of the mitochondrial iron–sulfur cluster assembly machinery. *Sci. Rep.*, **9**, 18986.
53. Camaschella, C., Campanella, A., De Falco, L., Boschetto, L., Merlini, R., Silvestri, L., Levi, S. and Iolascon, A. (2007) The human counterpart of zebrafish shiraz shows sideroblastic-like microcytic anemia and iron overload. *Blood*, **110**, 1353–1358.
54. Ye, H., Jeong, S.Y., Ghosh, M.C., Kovtunovych, G., Silvestri, L., Ortillo, D., Uchida, N., Tisdale, J., Camaschella, C. and Rouault, T.A. (2010) Glutaredoxin 5 deficiency causes sideroblastic anemia by specifically impairing heme biosynthesis and depleting cytosolic iron in human erythroblasts. *J. Clin. Invest.*, **120**, 1749–1761.
55. Liu, G., Guo, S., Anderson, G.J., Camaschella, C., Han, B. and Nie, G. (2014) Heterozygous missense mutations in the GLRX5 gene cause sideroblastic anemia in a Chinese patient. *Blood*, **124**, 2750–2751.
56. Lanz, N.D. and Booker, S.J. (2015) Auxiliary iron–sulfur cofactors in radical SAM enzymes. *BBA-Mol. Cell Res.*, **1853**, 1316–1334.
57. Wesley, N.A., Wachnowsky, C., Fidai, I. and Cowan, J.A. (2017) Analysis of NFU-1 metallocofactor binding-site substitutions-impacts on iron–sulfur cluster coordination and protein structure and function. *FEBS J.*, **284**, 3817–3837.
58. McCarthy, E.L. and Booker, S.J. (2018) Chapter eight—biochemical approaches for understanding iron–sulfur cluster regeneration in *Escherichia coli* lipoyl synthase during catalysis. In Bandarian, V. (ed), *Methods in Enzymology*. Academic Press, **606**: pp. 217–239.
59. Chaperon, D.-N. (2006) Construction and complementation of in-frame deletions of the essential *Escherichia coli* thymidylate kinase gene. *Appl. Environ. Microbiol.*, **72**, 1288–1294.
60. Nelson, C.E. and Gardner, J.G. (2015) In-frame deletions allow functional characterization of complex cellulose degradation phenotypes in Cellvibrio japonicus. *Appl. Environ. Microbiol.*, **81**, 5968–5975.